MSC-07236

NASA TECHNICAL MEMORANDUM

NASA TM X-58098
October 1972

THE STAGING DYNAMICS OF A PROPOSED SPACE SHUTTLE CONFIGURATION

A Thesis Presented to the
Faculty of the Graduate School of the
University of Houston
in Partial Fulfillment of the
Requirements for the Degree of
Master of Science in Mechanical Engineering

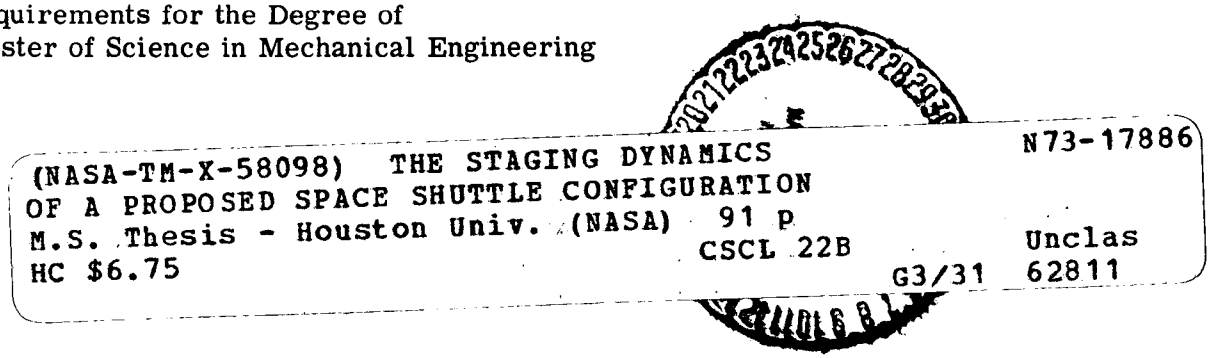

NATIONAL AERONAUTICS AND SPACE ADMINISTRATION

MANNED SPACECRAFT CENTER

HOUSTON, TEXAS 77058

1. Report No.	2. Government Accession No.	3. Recipient's Catalog No.
NASA TM X-58098		

4. Title and Subtitle	5. Report Date
THE STAGING DYNAMICS OF A PROPOSED SPACE SHUTTLE CONFIGURATION	October 1972
	6. Performing Organization Code

7. Author(s)	8. Performing Organization Report No.
David A. Hamilton, MSC	MSC-07236
	10. Work Unit No.
9. Performing Organization Name and Address	986-15-31-06-72
Manned Spacecraft Center Houston, Texas 77058	11. Contract or Grant No.
	13. Type of Report and Period Covered
12. Sponsoring Agency Name and Address	Technical Memorandum
National Aeronautics and Space Administration Washington, D.C. 20546	14. Sponsoring Agency Code

15. Supplementary Notes

16. Abstract

A mathematical model was developed to simulate the staging dynamics of a proposed space shuttle configuration. Included in the mathematical model is the kinematics and dynamics of the staging mechanism, thrust forces and thrust vector control, rigid-body dynamics, and structural dynamics of both the booster and orbiter stages of the configuration. The mathematical model was incorporated into a computer program so that the staging maneuver could be simulated. Results of the simulations are presented.

17. Key Words (Suggested by Author(s))	18. Distribution Statement
• Dynamics • Separation Dynamics • Digital Simulation • Vector Analysis • Structural Dynamics	

19. Security Classif. (of this report)	20. Security Classif. (of this page)	21. No. of Pages	22. Price
None	None	92	

NASA TM X-58098

THE STAGING DYNAMICS OF A PROPOSED SPACE SHUTTLE CONFIGURATION

David A. Hamilton
Manned Spacecraft Center
Houston, Texas 77058

III

Preceding page blank

CONTENTS

TABLES

FIGURES

THE STAGING DYNAMICS OF A PROPOSED SPACE SHUTTLE CONFIGURATION

By David A. Hamilton
Manned Spacecraft Center

SUMMARY

A mathematical model of the staging dynamics of a proposed space shuttle configuration was developed to evaluate a ram-activated linkage separation mechanism. Included in this model was the kinematics and dynamics of the staging mechanism, thrust forces, thrust vector control, rigid-body dynamics, and structural dynamics of both the booster and orbiter stages of the configuration. The model was incorporated into a computer program so that the staging maneuver could be simulated. The results of simulations of the staging maneuver demonstrated that the link-ram separation device provides satisfactory separation at nominal staging conditions.

INTRODUCTION

In an attempt to economize the U.S. space program, a completely reusable earth orbital launch vehicle has been under consideration by the National Aeronautics and Space Administration (NASA). One concept of this vehicle is a two-stage configuration in which the upper stage, the orbiter, is mounted "piggyback" on the lower stage, the booster. Both the booster and orbiter are winged vehicles. The configuration makes a vertical, rocket-type ascent, and each vehicle makes a horizontal, airplane-type descent. The booster delivers the orbiter to a desired altitude, then separates, flies back to earth, and lands. The orbiter continues thrusting until earth orbit is achieved.

The separation of the orbiter from the booster is a critical maneuver. The maneuver must occur safely, that is, the linear and angular motion of each vehicle must be such that no recontact between the vehicles occurs, and excessive heating because of engine plume impingement should not occur. A separation mechanism must be designed that will ensure safe separation. The loads generated on each vehicle by the mechanism must be within design limits, and the operation of the mechanism must be such that orbiter velocity losses during the maneuver are as small as possible.

Many candidate separation mechanisms have been proposed by NASA and support contractors. Because the testing of all proposed mechanisms is impractical, they are evaluated primarily by analytical techniques. These techniques involve developing mathematical models of the staging system. The models include the equations of motion of the booster and orbiter and the analytic description of the various forcing

/

functions that affect the motion of each vehicle. The mathematical model is usually incorporated into a computer simulation so that the staging maneuver can be simulated.

This thesis is concerned with the development of a mathematical model for predicting the interaction dynamics of the booster and orbiter during the separation sequence for a ram-activated linkage separation mechanism.

The link-ram system was not selected as the prime system by any of the NASA support contractors; thus, only limited analyses were conducted to evaluate it. The development in this thesis differs from previous analyses in that it includes modeling of the full six-degree-of-freedom motion of each vehicle, the structural representation of each link member, and the structural response of the booster and orbiter.

The mathematical techniques utilized in modeling the separation dynamics of the "piggyback" shuttle configuration are also applicable to the parallel burn shuttle configurations being considered by NASA.

SYMBOLS

A	link cross-sectional area
$\overrightarrow{BEV}$	vector location of booster engine
[BMG], [OMG]	matrix of natural frequencies of each vehicle
$\overrightarrow{BRMV}_1$	force vector on booster produced by ram mechanism 1
$\overrightarrow{BRMV}_2$	force vector on booster produced by ram mechanism 2
CX, CY, CZ	effective velocity gains
DLX_i	axial deflection of ith link member
DLY_i	lateral deflection of ith link member
DLY_{R1}	lateral deflection of ram mechanism 1
DTB1, DTB2, DTB3	booster Euler angle errors
DX, DY, DZ	gimbal command gains
EBX, EBY, EBZ	booster error signals
EBXI, EBYI, EBZI	booster error signal integrals
E	modulus of elasticity of link members

ETBX, ETBY, ETBZ	booster coordinate system components of Euler angle errors
F1, F2, F7, F8	forces acting at end points of link element
FBE	external forces acting on booster
$\overrightarrow{FLB_i}$	force vector at booster ith link attach point from link deflections
$\overrightarrow{FLKB}$	total force on booster from link forces
$\overrightarrow{FLKO}$	total force on orbiter from link forces
$\overrightarrow{FLO_i}$	force vector at orbiter ith link attach point from link deflections
FRAM	magnitude of ram force
$\overrightarrow{FRB_1}$	lateral force vector on booster from ram mechanism 1
$\overrightarrow{FRB_2}$	lateral force vector on booster from ram mechanism 2
FRM	maximum magnitude of ram force
$\overrightarrow{FRO_1}$	lateral force vector on orbiter from ram mechanism 1
$\overrightarrow{FRO_2}$	lateral force vector on orbiter from ram mechanism 2
FRY_1	lateral force on orbiter from ram mechanism 1
$\overrightarrow{FSMB}$	total force vector on booster
$\overrightarrow{FSMO}$	total force vector on orbiter
G	shear modulus of elasticity of link element
$GBCX_j$, $GBCY_j$, $GBCZ_j$	gimbal angle commands of jth booster engine
$[GBE(I, J)]_j$	transformation matrix from booster to jth booster engine coordinate system
[GBEA]	booster Euler rate transformation matrix
$[GBL(I, J)]_i$	transformation matrix from booster to ith booster link coordinate system
$[GBOL(I, J)]_i$	transformation matrix from ith booster link to ith orbiter link coordinate system

$GBXD_j$, $GBYD_j$, $GBZD_j$	gimbal rate commands of jth booster engine
[GIB(I, J)]	transformation matrix from inertial to booster coordinate system
[GIO(I, J)]	transformation matrix from inertial to orbiter coordinate system
$[GOE(I, J)]_j$	transformation matrix from orbiter to jth orbiter engine coordinate system
[GOEA(I, J)]	orbiter Euler rate transformation matrix
$[GOL(I, J)]_i$	transformation matrix from orbiter to ith orbiter link coordinate system
I	cross-sectional moment of inertia of link element
[INRB(I, J)]	inertia matrix of booster
[INRO(I, J)]	inertia matrix of orbiter
IXXB, IYYB, IZZB	booster moments of inertia
IXYB, IXZB, IYZB	booster products of inertia
IXXO, IYYO, IZZO	orbiter moments of inertia
IXYO, IXZO, IYZO	orbiter products of inertia
$\bar{i}, \bar{j}, \bar{k}$	unit vectors along X-, Y-, Z-axes
J	polar moment of inertia of link element
KRL	lateral stiffness of ram mechanism 1
KRR	engine roll control constant
ℓ	length of link element
[MBG], [MOG]	generalized mass matrix of each vehicle
MBT	total booster mass
MOT	total orbiter mass
M_1	number of booster engines
M_2	number of orbiter engines
OEV	vector location of orbiter engine

$\overrightarrow{ORMV}_1$	force on orbiter produced by ram mechanism 1
$\overrightarrow{ORMV}_2$	force on orbiter produced by ram mechanism 2
$\overrightarrow{PBSR}_1$	vector from booster center of gravity (c.g.) to ram 1 attach point on booster
$\overrightarrow{PBSR}_2$	vector from booster c.g. to ram 2 attach point on booster
$\overrightarrow{POSB}_i$	vector from booster c.g. to ith link attach point on booster
$\overrightarrow{POSO}_i$	vector from orbiter c.g. to ith attach point on orbiter
$\overrightarrow{POSR}_1$	vector from orbiter c.g. to ram 1 attach point on orbiter
$\overrightarrow{POSR}_2$	vector from orbiter c.g. to ram 2 attach point on orbiter
RX, RY, RZ	angular rate gyro gains
$\overrightarrow{SB}$	inertial position vector of booster c.g.
$\overrightarrow{SBD}_i$	booster structural deflection vector at ith link attach point
$\overrightarrow{SBD}_{R1}$	booster structural deflection at ram 1 attach point
$\overrightarrow{SBD}_{R2}$	booster structural deflection at ram 2 attach point
$\overrightarrow{SBO}$	vector from booster c.g. to orbiter c.g.
$\overrightarrow{SEPV}_i$	vector along ith link from booster to orbiter attach point
$\overrightarrow{SO}$	inertial position vector of orbiter c.g.
$\overrightarrow{SOD}_i$	orbiter structural deflection vector at ith link attach point
$\overrightarrow{SOD}_{R1}$	orbiter structural deflection at ram 1 attach point
$\overrightarrow{SOD}_{R2}$	orbiter structural deflection at ram 2 attach point
$SPXI_i$	initial axial length of ith link
$\overrightarrow{SRM}_1$	vector along ram 1 from booster to orbiter attach point
SYI_1	initial lateral deflection of ram mechanism 1

T4, T6, T10, T12	torques acting at end points of link element
$\overrightarrow{TBRM_1}$	torque vector on booster c.g. produced by ram mechanism 1
$\overrightarrow{TBRM_2}$	torque vector on booster c.g. produced by ram mechanism 2
$\overrightarrow{THMB}$	total thrust torque vector on booster c.g.
$\overrightarrow{THMO}$	total thrust torque vector on orbiter c.g.
$\overrightarrow{THRVB}$	total thrust vector on booster
$\overrightarrow{THRVO}$	total thrust vector on orbiter
$\overrightarrow{TLB_i}$	torque vector at booster ith link attach point from link rotations
$\overrightarrow{TLKB}$	total torque on booster c.g. from link forces
$\overrightarrow{TLKO}$	total torque on orbiter c.g. from link forces
$\overrightarrow{TLO_i}$	torque vector at orbiter ith link attach point from link rotations
TMAGB	magnitude of booster thrust
TMAGO	magnitude of orbiter thrust
$\overrightarrow{TMB}$	total torque vector about booster c.g.
$\overrightarrow{TMO}$	total torque vector about orbiter c.g.
$\overrightarrow{TORM_1}$	torque vector on orbiter c.g. produced by ram mechanism 1
$\overrightarrow{TORM_2}$	torque vector on orbiter c.g. produced by ram mechanism 2
$\overrightarrow{TRB_1}$	torque at ram 1 attach point on booster
$\overrightarrow{TRB_2}$	torque at ram 2 attach point on booster
Tsep	release time of separation sequence
Tswing	time to initiate swing phase of separation sequence
t	time
U1, U2, U4, U6	displacements at end points of link element

U7, U8, U10, U12	rotations at end points of link element
$\overrightarrow{VEB}_j$	vector from booster c.g. to ith booster engine
$\overrightarrow{VEO}_j$	vector from orbiter c.g. to ith booster engine
XI, YI, ZI	error signal integrator gains
$\Delta\theta BL$	link-swing angle
ζ	percent of critical damping
$\theta BE_j'$, $\theta OE_j'$	pitch angles of booster and orbiter engines with roll control included
θBL_i	Euler angle from booster to ith booster link coordinate system
θOL_i	Euler angle from orbiter to ith orbiter link coordinate system
λ	constant used in ram force relation
ξB	generalized displacements of booster
ξO	generalized displacements of orbiter
$[\phi B]$, $[\phi O]$	booster and orbiter modal matrices
ϕBE_j, ϕOE_j	hypothetical roll angles of booster and orbiter jth engines
ψB, θB, ϕB	Euler angles of inertial to booster coordinate system
ψB_c, θB_c, ϕB_c	booster commanded Euler angles
ψBE_j, θBE_j	gimbal angles of jth booster engine
ψL_i, ϕL_i, θL_i	relative rotation of end points of ith link member
ψO, θO, ϕO	Euler angles of inertial to orbiter coordinate system
ψOE_j, θOE_j	gimbal angles of jth booster engine
$\overrightarrow{\omega B}$	angular velocity vector of booster
$\overrightarrow{\omega O}$	angular velocity of orbiter

Modifying Symbols:

B	refers to booster quantity
B_j, BE_j	refers to jth booster engine
BL_i	refers to ith link relative to booster
I	refers to the initial values of various quantities
i	refers to ith link member
j	refers to engines on each vehicle
O	refers to orbiter quantity
OE_j	refers to jth orbiter engine
OL_i	refers to ith link relative to orbiter
X, Y, Z	body axes of either booster or orbiter

Operators:

$[\,]^{-1}$	inverse of a matrix
$[\,]^{T}$	transpose of a matrix
$(\dot{})$	first derivative with respect to time, $\frac{d(\,)}{dt}$
$(\ddot{})$	second derivative with respect to time, $\frac{d^2(\,)}{dt^2}$

GENERAL DESCRIPTION OF THE STAGING MECHANISM AND THE STAGING SEQUENCE

The Staging Mechanism

The link-ram separation system, which is modeled in this thesis, is divided into two identical sections. The relative location of these sections is illustrated in figure 1(a), and a perspective view of one section is shown in figure 1(b). Each section is composed of two standoff links, two parallel swing links, and a ram mechanism (fig. 1(b)). The standoff links in both sections and the swing links in the forward section carry all loads between the two vehicles prior to the staging maneuver. The

swing-link members in both sections provide a constraint between the booster and orbiter during the swing phase of the separation maneuver, and the ram mechanisms produce a separation force between the vehicles during this phase. The standoff and swing links are pinned parallel to the Y-axis of each vehicle. The ram mechanisms are pinned parallel to the Y-axis of the booster and have ball-joint attachments on the orbiter.

The Staging Sequence

The nominal staging maneuver for the shuttle configuration being modeled (ref. 1) occurs at an approximate altitude of 68 885 meters, and the staging velocity is approximately 2743 m/sec. The staging sequence is initiated by throttling down the booster engines and simultaneously throttling up the orbiter engines as illustrated in figure 2. When both vehicles are at the desired thrust levels, the swing phase of the staging sequence begins. At this time, the forward and aft standoff links (fig. 1(b)) are pyrotechnically released from the orbiter, and the ram mechanisms are simultaneously activated. The standoff links are retracted into the booster for the duration of the flight. During the swing phase of the staging sequence, the orbiter moves forward relative to the booster. This relative motion occurs primarily because the thrust-to-weight ratio of the orbiter is greater than that of the booster, but the ram forces also contribute significantly to the relative velocity between vehicles.

The duration of the swing phase is scheduled according to time or to link-swing angles, whichever achieves its preset maximum value first. At the end of the swing phase, the swing links are pyrotechnically disconnected, and the ram mechanisms are mechanically disconnected from the orbiter. Both the swing links and ram mechanisms are drawn back into the booster for the duration of the flight.

GENERAL DISCUSSION OF THE MATHEMATICAL MODEL

The formulation of the mathematical model for computing the booster/orbiter staging dynamics starts with the determining of the governing equations of motion of each vehicle. In this model, each vehicle is given the full six degree of freedom, that is, three degrees in translation and three degrees in rotation. The governing translational equations of motion are obtained from Newton's second law, and the governing rotational equations are from Euler's moment equations.

The total forces and torques on each vehicle that are used in the governing equations were assumed to be affected by booster and orbiter thrust, interaction link dynamics, ram-mechanism dynamics, and structural dynamics. To facilitate calculation of the various forces acting on the booster and orbiter, multiple coordinate systems are used in this mathematical model. These coordinate systems define the orientation of the booster, booster engines, orbiter, orbiter engines, and link elements.

To calculate the link forces, each link member is idealized as a beam element. The stiffness characteristics for the links are developed, and the forces from the link

dynamics are calculated from the linear and angular deflections of the ends of each link. The link forces are coupled with the structural response of each vehicle by the vehicle response at the link attach points.

The structural response of each vehicle is calculated from the respective modal characteristics of the vehicle and from the thrust, link, and ram forces. This response is, in turn, used to calculate vehicle displacements at link, ram, and engine attach points.

The ram mechanism forces are governed by the magnitude of the force generated by the ram and by the orientation of the ram between the booster and orbiter.

The engine thrust vector on each vehicle is a function of the thrust magnitude and the thrust vector control (TVC) logic. The TVC logic determines the engine gimbal angles based on desired attitude, and the thrust magnitude is controlled by desired thrust scheduling.

This mathematical model was incorporated into a computer program so that the staging sequence could be simulated as a function of time. All differential equations were numerically integrated in the computer program using an Adams-Moulton predictor corrector with a Runge-Kutta starter. The general sequencing of the mathematical model is illustrated by the computer program flow chart given in figure 3. The formulation of the mathematical model of the staging sequence is discussed in more detail in the following chapters.

COORDINATE SYSTEMS AND TRANSFORMATIONS

The various coordinate systems used in the mathematical model are illustrated in figures 4 and 5. All coordinate systems used are orthogonal, right-hand systems. The booster and orbiter systems are coincident with the inertial system at the beginning of the swing phase of the staging sequence. The engine and link systems on each vehicle are oriented relative to that vehicle.

Inertial Coordinate System

The inertial coordinate system is fixed with respect to booster and orbiter motion. The system is used to define the position and orientation of each vehicle by the position vectors $\vec{SB}$ and $\vec{SO}$ and the Euler angles ψB, θB, ϕB, and ψO, θO, ϕO.

The order of Euler angle rotation from the inertial to booster and orbiter coordinate systems is about the Z-, Y-, X-axes of the vehicle (fig. 6), and the coordinate transformation matrix that corresponds to these angles is defined as follows.

$$\begin{Bmatrix} \bar{i} \\ \bar{j} \\ \bar{k} \end{Bmatrix}_B = \begin{bmatrix} \\ GIB(I,J) \\ \\ \end{bmatrix} \begin{Bmatrix} \bar{i} \\ \bar{j} \\ \bar{k} \end{Bmatrix}_I \tag{1}$$

where $\bar{i}$, $\bar{j}$, and $\bar{k}$ are unit vectors along the respective system axes, and the elements of [GIB] are

$$
\begin{aligned}
GIB(1,1) &= COS(\theta B) \cdot COS(\psi B) \\
GIB(1,2) &= COS(\theta B) \cdot SIN(\psi B) \\
GIB(1,3) &= -SIN(\theta B) \\
GIB(2,1) &= -COS(\phi B) \cdot SIN(\psi B) + SIN(\phi B) \cdot SIN(\theta B) \cdot COS(\psi B) \\
GIB(2,2) &= COS(\phi B) \cdot COS(\psi B) + SIN(\phi B) \cdot SIN(\theta B) \cdot SIN(\psi B) \\
GIB(2,3) &= SIN(\phi B) \cdot COS(\theta B) \\
GIB(3,1) &= SIN(\phi B) \cdot SIN(\psi B) + COS(\phi B) \cdot SIN(\theta B) \cdot COS(\psi B) \\
GIB(3,2) &= -SIN(\phi B) \cdot COS(\psi B) + COS(\phi B) \cdot SIN(\theta B) \cdot SIN(\psi B) \\
GIB(3,3) &= COS(\phi B) \cdot COS(\theta B)
\end{aligned}
\tag{2}
$$

Also,

$$
\begin{Bmatrix} \bar{i} \\ \bar{j} \\ \bar{k} \end{Bmatrix}_O = \begin{bmatrix} GIO(I,J) \end{bmatrix} \begin{Bmatrix} \bar{i} \\ \bar{j} \\ \bar{k} \end{Bmatrix}_I \tag{3}
$$

where the elements of [GIO] are defined in the same manner as [GIB] using the orbiter Euler angles. Because these Euler angle transformation matrices are orthogonal, then

$$
[GIB]^{-1} = [GIB]^T \tag{4}
$$

from which

$$
\begin{Bmatrix} \bar{i} \\ \bar{j} \\ \bar{k} \end{Bmatrix}_I = \begin{bmatrix} GIB(I,J) \end{bmatrix}^T \begin{Bmatrix} \bar{i} \\ \bar{j} \\ \bar{k} \end{Bmatrix}_B \tag{5}
$$

The Euler angle rate transformation matrix is used to relate vehicle angular velocities to the Euler angle rates, that is,

$$\begin{Bmatrix} \dot{\psi}B \\ \dot{\theta}B \\ \dot{\phi}B \end{Bmatrix} = \begin{bmatrix} \\ GBEA(I,J) \\ \\ \end{bmatrix} \begin{Bmatrix} \omega BX \\ \omega BY \\ \omega BZ \end{Bmatrix} \tag{6}$$

where the elements of [GBEA] are defined as follows.

$$\begin{aligned} GBEA(1,1) &= 0 \\ GBEA(1,2) &= SIN(\phi B)/COS(\theta B) \\ GBEA(1,3) &= COS(\phi B)/COS(\theta B) \\ GBEA(2,1) &= 0 \\ GBEA(2,2) &= COS(\phi B) \\ GBEA(2,3) &= -SIN(\phi B) \\ GBEA(3,1) &= 1 \\ GBEA(3,2) &= TAN(\theta B) \cdot SIN(\phi B) \\ GBEA(3,3) &= TAN(\theta B) \cdot COS(\phi B) \end{aligned} \tag{7}$$

Likewise, the orbiter Euler angle rates are related to the orbiter angular velocities by

$$\begin{Bmatrix} \dot{\psi}O \\ \dot{\theta}O \\ \dot{\phi}O \end{Bmatrix} = \begin{bmatrix} \\ GOEA(I,J) \\ \\ \end{bmatrix} \begin{Bmatrix} \omega OX \\ \omega OY \\ \omega OZ \end{Bmatrix} \tag{8}$$

where the elements of [GOEA] are defined in the same manner as [GBEA] using the orbiter Euler angles.

Engine Coordinate Systems

The engines on both booster and orbiter are positioned at the engine gimbal point and are oriented relative to the respective vehicle coordinate system. Each engine is

restricted to rotation about two axes because rotation about the roll (X) axis would not produce vehicle control. Thus, the coordinate transformation matrix from the booster to the jth booster engine is

$$\begin{Bmatrix} \bar{i} \\ \bar{j} \\ \bar{k} \end{Bmatrix}_{BE_j} = \left[GBE(I,J) \right]_j \begin{Bmatrix} \bar{i} \\ \bar{j} \\ \bar{k} \end{Bmatrix}_B \tag{9}$$

where the elements of $[GBE]_j$ are as follows.

$$\begin{aligned}
GBE(1,1)_j &= COS(\theta BE_j) \cdot COS(\psi BE_j) \\
GBE(1,2)_j &= COS(\theta BE_j) \cdot SIN(\psi BE_j) \\
GBE(1,3)_j &= -SIN(\theta BE_j) \\
GBE(2,1)_j &= -SIN(\psi BE_j) \\
GBE(2,2)_j &= COS(\psi BE_j) \\
GBE(2,3)_j &= 0 \\
GBE(3,1)_j &= SIN(\theta BE_j) \cdot COS(\psi BE_j) \\
GBE(3,2)_j &= SIN(\theta BE_j) \cdot SIN(\psi BE_j) \\
GBE(3,3)_j &= COS(\theta BE_j)
\end{aligned} \tag{10}$$

Also,

$$\begin{Bmatrix} \bar{i} \\ \bar{j} \\ \bar{k} \end{Bmatrix}_{OE_j} = \left[GOE(I,J) \right]_j \begin{Bmatrix} \bar{i} \\ \bar{j} \\ \bar{k} \end{Bmatrix}_O \tag{11}$$

where the elements of $[GOE]_j$ are defined in the same manner as $[GBE]_j$ using the orbiter engine Euler angles.

Link Coordinate Systems

The link coordinate systems are located at the booster and orbiter attach point of each link. The system at each end is oriented with respect to the coordinate system of the vehicle to which it is attached. Because each link member is pinned parallel to the Y-axis of the attached vehicle, the link coordinate system is free to rotate only about the Y-axis of that vehicle. Thus, the coordinate transformation matrix from booster to the ith booster link coordinate system is

$$\begin{Bmatrix} \bar{i} \\ \bar{j} \\ \bar{k} \end{Bmatrix}_{BL_i} = \begin{bmatrix} GBL(I,J) \end{bmatrix}_i \begin{Bmatrix} \bar{i} \\ \bar{j} \\ \bar{k} \end{Bmatrix}_B \tag{12}$$

where the elements of $[GBL]_i$ are

$$\begin{aligned} GBL(1,1)_i &= COS(\theta BL_i) \\ GBL(1,2)_i &= 0 \\ GBL(1,3)_i &= -SIN(\theta BL_i) \\ GBL(2,1)_i &= 0 \\ GBL(2,2)_i &= 1 \\ GBL(2,3)_i &= 0 \\ GBL(3,1)_i &= SIN(\theta BL_i) \\ GBL(3,2)_i &= 0 \\ GBL(3,3)_i &= COS(\theta BL_i) \end{aligned} \tag{13}$$

Also,

$$\begin{Bmatrix} \bar{i} \\ \bar{j} \\ \bar{k} \end{Bmatrix}_{OL_i} = \begin{bmatrix} GOL(I,J) \end{bmatrix}_i \begin{Bmatrix} \bar{i} \\ \bar{j} \\ \bar{k} \end{Bmatrix}_O \tag{14}$$

where the elements of $[GOL]_i$ are defined in the same manner as $[GBL]_i$ using the orbiter link rotation θOL_i.

VEHICLE EQUATIONS OF MOTION

The equations of motion for the booster and orbiter are obtained from Newton's second law for translation and from Euler's moment equations for rotation.

The elementary equations of translation for each vehicle in component form are

$$\begin{Bmatrix} \ddot{SBX} \\ \ddot{SBY} \\ \ddot{SBZ} \end{Bmatrix} = \frac{1}{MBT} \begin{Bmatrix} FSMBX \\ FSMBY \\ FSMBZ \end{Bmatrix} \tag{15}$$

and

$$\begin{Bmatrix} \ddot{SOX} \\ \ddot{SOY} \\ \ddot{SOZ} \end{Bmatrix} = \frac{1}{MOT} \begin{Bmatrix} FSMOX \\ FSMOY \\ FSMOZ \end{Bmatrix} \tag{16}$$

where FSMBX, FSMBY, FSMBZ and FSMOX, FSMOY, FSMOZ are the components of the total external forces on each vehicle, respectively.

Euler's moment equations for rotational motion for the booster (refs. 2 and 3) are

$$\begin{Bmatrix} TMBX \\ TMBY \\ TMBZ \end{Bmatrix} = \begin{bmatrix} \\ INRB(I,J) \\ \\ \end{bmatrix} \begin{Bmatrix} \dot{\omega BX} \\ \dot{\omega BY} \\ \dot{\omega BZ} \end{Bmatrix} + \begin{bmatrix} 0 & -\omega BZ & \omega BY \\ \omega BZ & 0 & -\omega BX \\ -\omega BY & \omega BX & 0 \end{bmatrix} \begin{bmatrix} \\ INRB(I,J) \\ \\ \end{bmatrix} \begin{Bmatrix} \omega BX \\ \omega BY \\ \omega BZ \end{Bmatrix} \tag{17}$$

where TMBX, TMBY, TMBZ are the components of the total torque vector on the booster c.g.

The elements of [INRB] are

$$
\begin{aligned}
&INRB(1,1) = IXXB \\
&INRB(1,2) = -IXYB \\
&INRB(1,3) = -IXZB \\
&INRB(2,1) = -IXYB \\
&INRB(2,2) = IYYB \\
&INRB(2,3) = -IYZB \\
&INRB(3,1) = -IXZB \\
&INRB(3,2) = -IYZB \\
&INRB(3,3) = IZZB
\end{aligned}
\tag{18}
$$

Similarly, Euler's moment equations for the orbiter are

$$
\begin{Bmatrix} TMOX \\ TMOY \\ TMOZ \end{Bmatrix} = \begin{bmatrix} \\ INRO(I,J) \\ \\ \end{bmatrix} \begin{Bmatrix} \dot{\omega OX} \\ \dot{\omega OY} \\ \dot{\omega OZ} \end{Bmatrix} + \begin{bmatrix} 0 & -\omega OZ & \omega OY \\ \omega OZ & 0 & -\omega OX \\ -\omega OY & \omega OX & 0 \end{bmatrix} \begin{bmatrix} \\ INRO(I,J) \\ \\ \end{bmatrix} \begin{Bmatrix} \omega OX \\ \omega OY \\ \omega OZ \end{Bmatrix} \tag{19}
$$

where the elements of [INRO] are defined in the same manner as [INRB] using the orbiter inertias.

The translational equations of motion can be integrated with respect to time to yield the booster and orbiter inertial velocities. Likewise, these velocities can be integrated to yield the corresponding displacements of each vehicle.

$$
\begin{Bmatrix} \dot{SBX} \\ \dot{SBY} \\ \dot{SBZ} \end{Bmatrix} = \int \begin{Bmatrix} \ddot{SBX} \\ \ddot{SBY} \\ \ddot{SBZ} \end{Bmatrix} dt + \begin{Bmatrix} \dot{SBX}_I \\ \dot{SBY}_I \\ \dot{SBZ}_I \end{Bmatrix} \tag{20}
$$

and

$$\begin{Bmatrix} S\dot{O}X \\ S\dot{O}Y \\ S\dot{O}Z \end{Bmatrix} = \int \begin{Bmatrix} S\ddot{O}X \\ S\ddot{O}Y \\ S\ddot{O}Z \end{Bmatrix} dt + \begin{Bmatrix} S\dot{O}X_I \\ S\dot{O}Y_I \\ S\dot{O}Z_I \end{Bmatrix} \tag{21}$$

also

$$\begin{Bmatrix} SBX \\ SBY \\ SBZ \end{Bmatrix} = \int \begin{Bmatrix} S\dot{B}X \\ S\dot{B}Y \\ S\dot{B}Z \end{Bmatrix} dt + \begin{Bmatrix} SBX_I \\ SBY_I \\ SBZ_I \end{Bmatrix} \tag{22}$$

and

$$\begin{Bmatrix} SOX \\ SOY \\ SOZ \end{Bmatrix} = \int \begin{Bmatrix} S\dot{O}X \\ S\dot{O}Y \\ S\dot{O}Z \end{Bmatrix} dt + \begin{Bmatrix} SOX_I \\ SOY_I \\ SOZ_I \end{Bmatrix} \tag{23}$$

The rotational equations (17) and (19) can be solved for $\dot{\vec{\omega}}\vec{B}$ and $\dot{\vec{\omega}}\vec{O}$, respectively. These vehicle angular accelerations can be integrated with respect to time to yield vehicle angular velocities, that is,

$$\begin{Bmatrix} \omega BX \\ \omega BY \\ \omega BZ \end{Bmatrix} = \int \begin{Bmatrix} \omega \dot{B}X \\ \omega \dot{B}Y \\ \omega \dot{B}Z \end{Bmatrix} dt + \begin{Bmatrix} \omega BX_I \\ \omega BY_I \\ \omega BZ_I \end{Bmatrix} \tag{24}$$

and

$$\begin{Bmatrix} \omega OX \\ \omega OY \\ \omega OZ \end{Bmatrix} = \int \begin{Bmatrix} \omega \dot{O}X \\ \omega \dot{O}Y \\ \omega \dot{O}Z \end{Bmatrix} dt + \begin{Bmatrix} \omega OX_I \\ \omega OY_I \\ \omega OZ_I \end{Bmatrix} \tag{25}$$

The vehicle angular velocities can be transferred into Euler angle rates (ref. 2) by the transformation matrix of equations (6) and (8), that is,

$$\begin{Bmatrix} \dot{\psi}B \\ \dot{\theta}B \\ \dot{\phi}B \end{Bmatrix} = \begin{bmatrix} \\ GBEA(I,J) \\ \\ \end{bmatrix} \begin{Bmatrix} \omega BX \\ \omega BY \\ \omega BZ \end{Bmatrix} \tag{26}$$

and

$$\begin{Bmatrix} \dot{\psi}O \\ \dot{\theta}O \\ \dot{\phi}O \end{Bmatrix} = \begin{bmatrix} \\ GOEA(I,J) \\ \\ \end{bmatrix} \begin{Bmatrix} \omega OX \\ \omega OY \\ \omega OZ \end{Bmatrix} \tag{27}$$

The Euler angle rates can then be integrated with respect to time to yield the booster and orbiter Euler angles, that is,

$$\begin{Bmatrix} \theta B \\ \psi B \\ \phi B \end{Bmatrix} = \int \begin{Bmatrix} \dot{\theta}B \\ \dot{\psi}B \\ \dot{\phi}B \end{Bmatrix} dt + \begin{Bmatrix} \theta B_I \\ \psi B_I \\ \phi B_I \end{Bmatrix} \tag{28}$$

and

$$\begin{Bmatrix} \theta O \\ \psi O \\ \phi O \end{Bmatrix} = \int \begin{Bmatrix} \dot{\theta}O \\ \dot{\psi}O \\ \dot{\phi}O \end{Bmatrix} dt + \begin{Bmatrix} \theta O_I \\ \psi O_I \\ \phi O_I \end{Bmatrix} \tag{29}$$

Thus, the position and orientation of the booster and orbiter at any time can be determined by knowledge of the external forces acting on the respective vehicles.

As previously mentioned, these external forces are affected by link and ram dynamics and the thrust of each vehicle. The total force vectors on each vehicle are

$$\overrightarrow{FSMB} = \overrightarrow{FLKB} + \overrightarrow{BRMV} + \overrightarrow{THRVB} \tag{30}$$

and

$$\overrightarrow{FSMO} = \overrightarrow{FLKO} + \overrightarrow{ORMV} + \overrightarrow{THRVO} \tag{31}$$

where $\overrightarrow{FLKB}$ and $\overrightarrow{FLKO}$ are total link forces, $\overrightarrow{BRMV}$ and $\overrightarrow{ORMV}$ are total ram forces, and $\overrightarrow{THRVB}$ and $\overrightarrow{THRVO}$ are total thrust forces on the booster and orbiter, respectively.

The corresponding total torques acting on each vehicle are

$$\overrightarrow{TMB} = \overrightarrow{TLKB} + \overrightarrow{TBRM} + \overrightarrow{THMB} \tag{32}$$

and

$$\overrightarrow{TMO} = \overrightarrow{TLKO} + \overrightarrow{TORM} + \overrightarrow{THMO} \tag{33}$$

where $\overrightarrow{TLKB}$ and $\overrightarrow{TLKO}$ are total link torques, $\overrightarrow{TBRM}$ and $\overrightarrow{TORM}$ are total ram torques, and $\overrightarrow{THMB}$ and $\overrightarrow{THMO}$ are total thrust torques on the booster and orbiter centers of gravity, respectively.

The development of the various forces and torques acting on the booster and orbiter is discussed in the following sections.

LINK FORCES

The forces generated in each link element are calculated from the translational and rotational displacements at each end of the link element and from the corresponding stiffness characteristics of that element.

The translational displacements of each link element are calculated as follows. The vector $\overrightarrow{SEPV}_i$ (fig. 7) between the booster ith link attach point and the corresponding orbiter ith attach point is calculated from vector loop equations. A vector from the booster c.g. to the orbiter ith link attach point can be written in two forms. Because the two equations define the same point from the same origin, they can be equated, that is,

$$\overrightarrow{POSB}_i + \overrightarrow{SBD}_i + \overrightarrow{SEPV}_i = \overrightarrow{SBO} + \overrightarrow{POSO}_i + \overrightarrow{SOD}_i \tag{34}$$

where $\overrightarrow{POSB}_i$ and $\overrightarrow{POSO}_i$ define the ith link attach point on each vehicle relative to its c.g. The vectors $\overrightarrow{SBD}_i$ and $\overrightarrow{SOD}_i$ are the structural displacements at the ith link attach point on each vehicle, respectively. The vector $\overrightarrow{SBO}$ defines the orbiter c.g. relative to the booster c.g. and is calculated from the inertial position vector of each vehicle, that is,

$$\overrightarrow{SB} + \overrightarrow{SBO} = \overrightarrow{SO} \tag{35}$$

or

$$\overrightarrow{SBO} = \overrightarrow{SO} - \overrightarrow{SB} \tag{36}$$

Equation (36) is substituted into equation (34), and solving for $\overrightarrow{SEPV}_i$ yields equation (37).

$$\overrightarrow{SEPV}_i = \overrightarrow{SO} - \overrightarrow{SB} + \overrightarrow{POSO}_i + \overrightarrow{SOD}_i - \overrightarrow{POSB}_i - \overrightarrow{SBD}_i \tag{37}$$

that defines the position of the ith link attach point on the orbiter with respect to the booster ith link attach point. This vector can be expressed in the link coordinate system, and then the deflections of that link can be directly calculated from the vector components, that is,

$$DLX_i = SEPVX_i(t) - SPXI_i \tag{38}$$

and

$$DLY_i = SEPVY_i(t) \tag{39}$$

The link deflection in the ZBL and ZOL direction (fig. 5) is zero because the link is pinned about the YBL and YOL axis.

The rotations of the end points of each link element are calculated as follows. Vectors in the booster, booster link, orbiter, orbiter link, and inertial coordinate systems are related according to equations (1), (12), (13), and (14), that is,

$$\begin{Bmatrix} \bar{i} \\ \bar{j} \\ \bar{k} \end{Bmatrix}_B = \begin{bmatrix} \\ GIB(I,J) \\ \\ \end{bmatrix} \begin{Bmatrix} \bar{i} \\ \bar{j} \\ \bar{k} \end{Bmatrix}_I \tag{40}$$

and

$$\begin{Bmatrix} \bar{i} \\ \bar{j} \\ \bar{k} \end{Bmatrix}_{BL_i} = \begin{bmatrix} \\ GBL(I,J) \\ \\ \end{bmatrix}_i \begin{Bmatrix} \bar{i} \\ \bar{j} \\ \bar{k} \end{Bmatrix}_B \tag{41}$$

and

$$\begin{Bmatrix} \bar{i} \\ \bar{j} \\ \bar{k} \end{Bmatrix}_O = \begin{bmatrix} \\ GIO(I,J) \\ \\ \end{bmatrix} \begin{Bmatrix} \bar{i} \\ \bar{j} \\ \bar{k} \end{Bmatrix}_I \tag{42}$$

and

$$\begin{Bmatrix} \bar{i} \\ \bar{j} \\ \bar{k} \end{Bmatrix}_{OL_i} = \begin{bmatrix} \\ GOL(I,J) \\ \\ \end{bmatrix}_i \begin{Bmatrix} \bar{i} \\ \bar{j} \\ \bar{k} \end{Bmatrix}_O \tag{43}$$

Equations (40) and (41) can be written as

$$\begin{Bmatrix} \bar{i} \\ \bar{j} \\ \bar{k} \end{Bmatrix}_I = \begin{bmatrix} \\ GIB(I,J) \\ \\ \end{bmatrix}^T \begin{Bmatrix} \bar{i} \\ \bar{j} \\ \bar{k} \end{Bmatrix}_B \tag{44}$$

and

$$\begin{Bmatrix} \bar{i} \\ \bar{j} \\ \bar{k} \end{Bmatrix}_B = \left[\text{GBL}(I,J) \right]_i^T \begin{Bmatrix} \bar{i} \\ \bar{j} \\ \bar{k} \end{Bmatrix}_{BL_i} \tag{45}$$

Equation (45) can be substituted into equation (44) to yield the coordinate transformation from the booster link to the inertial system, that is,

$$\begin{Bmatrix} \bar{i} \\ \bar{j} \\ \bar{k} \end{Bmatrix}_I = \left[\text{GIB}(I,J) \right]^T \left[\text{GBL}(I,J) \right]_i^T \begin{Bmatrix} \bar{i} \\ \bar{j} \\ \bar{k} \end{Bmatrix}_{BL_i} \tag{46}$$

This relation (eq. (46)) can then be substituted into equation (42) to yield equation (47) as given below.

$$\begin{Bmatrix} \bar{i} \\ \bar{j} \\ \bar{k} \end{Bmatrix}_O = \left[\text{GIO}(I,J) \right] \left[\text{GIB}(I,J) \right]^T \left[\text{GBL}(I,J) \right]_i^T \begin{Bmatrix} \bar{i} \\ \bar{j} \\ \bar{k} \end{Bmatrix}_{BL_i} \tag{47}$$

Equation (47) can then be substituted into (43) to yield the coordinate transformation from booster link to orbiter link coordinate systems, that is,

$$\begin{Bmatrix} \bar{i} \\ \bar{j} \\ \bar{k} \end{Bmatrix}_{OL_i} = \left[\text{GOL}(I,J) \right]_i \left[\text{GIO}(I,J) \right] \left[\text{GIB}(I,J) \right]^T \left[\text{GBL}(I,J) \right]_i^T \begin{Bmatrix} \bar{i} \\ \bar{j} \\ \bar{k} \end{Bmatrix}_{BL_i} \tag{48}$$

or

$$\begin{Bmatrix} \bar{i} \\ \bar{j} \\ \bar{k} \end{Bmatrix}_{OL_i} = \left[\text{GBOL}(I,J) \right]_i \begin{Bmatrix} \bar{i} \\ \bar{j} \\ \bar{k} \end{Bmatrix}_{BL_i} \tag{49}$$

where

$$[GBOL(I,J)]_i = [GOL(I,J)]_i[GIO(I,J)][GIB(I,J)]^T[GBL(I,J)]_i^T \tag{50}$$

Now the rotations of ith link at the orbiter attach point (link end II) with respect to its booster attach point (link end I) can be solved for by the ratio of certain elements of $[GBOL]_i$. The elements of $[GBOL]_i$ for Euler angle rotation order Z, Y, X are given below.

$$\begin{aligned}
GBOL(1,1)_i &= COS(\theta L_i) \cdot COS(\psi L_i) \\
GBOL(1,2)_i &= COS(\theta L_i) \cdot SIN(\psi L_i) \\
GBOL(1,3)_i &= -SIN(\theta L_i) \\
GBOL(2,1)_i &= -COS(\phi L_i) \cdot SIN(\psi L_i) + SIN(\phi L_i)SIN(\theta L_i)COS(\psi L_i) \\
GBOL(2,2)_i &= COS(\phi L_i)COS(\psi L_i) + SIN(\phi L_i)SIN(\theta L_i)SIN(\psi L_i) \\
GBOL(2,3)_i &= SIN(\phi L_i) \cdot COS(\theta L_i) \\
GBOL(3,1)_i &= SIN(\phi L_i)SIN(\psi L_i) + COS(\phi L_i)SIN(\theta L_i)COS(\psi L_i) \\
GBOL(3,2)_i &= -SIN(\phi L_i)COS(\psi L_i) + COS(\phi L_i)SIN(\theta L_i)SIN(\psi L_i) \\
GBOL(3,3)_i &= COS(\phi L_i)COS(\theta L_i)
\end{aligned} \tag{51}$$

from which

$$\begin{aligned}
\phi L_i &\doteq TAN^{-1}\left(GBOL(2,3)_i\right)/\left(GBOL(3,3)_i\right) \\
\psi L_i &= TAN^{-1}\left(GBOL(1,2)_i\right)/\left(GBOL(1,1)_i\right)
\end{aligned} \tag{52}$$

The link stiffness characteristics are calculated by idealizing each link member as a beam element. The boundary conditions for each link can then be applied to the general stiffness matrix of a beam element as given in reference 4 to yield the stiffness matrix of each link (appendix A). The translational and rotational displacements of the

ith link end II relative to end I can be multiplied by the corresponding link stiffness matrix to yield forces at the orbiter attach point, that is,

$$\begin{Bmatrix} FLOX_i \\ FLOY_i \\ TLOX_i \\ TLOZ_i \end{Bmatrix} = \begin{bmatrix} AE/\ell & 0 & 0 & 0 \\ 0 & 12EI/\ell^3 & 0 & -6EI/\ell^2 \\ 0 & 0 & JG/\ell & 0 \\ 0 & -6EI/\ell^2 & 0 & 4EI/\ell \end{bmatrix}_i \begin{Bmatrix} DLX_i \\ DLY_i \\ \phi L_i \\ \psi L_i \end{Bmatrix} \tag{53}$$

and the reaction forces on the booster are given in equation (54).

$$\begin{Bmatrix} FLBX \\ FLBY \\ TLBX \\ TLBZ \end{Bmatrix} = -\begin{Bmatrix} FLOX \\ FLOY \\ TLOX \\ TLOZ \end{Bmatrix} + \begin{Bmatrix} 0 \\ 0 \\ 0 \\ FLBY \cdot \ell \end{Bmatrix} \tag{54}$$

The total link forces and torques acting on each vehicle are the vector sum of the individual link forces and torques, that is,

$$\begin{aligned} \overrightarrow{FLKB} &= \sum_{i=1}^{N} \overrightarrow{FLB}_i \\ \overrightarrow{FLKO} &= \sum_{i=1}^{N} \overrightarrow{FLO}_i \end{aligned} \tag{55}$$

$$\begin{aligned} \overrightarrow{TLKB} &= \sum_{i=1}^{N} \overrightarrow{TLB}_i + \left(\overrightarrow{POSB}_i + \overrightarrow{SBD}_i\right) \times \overrightarrow{FLB}_i \\ \overrightarrow{TLKO} &= \sum_{i=1}^{N} \overrightarrow{TLO}_i + \left(\overrightarrow{POSO}_i + \overrightarrow{SOD}_i\right) \times \overrightarrow{FLO}_i \end{aligned} \tag{56}$$

RAM MECHANISM FORCES

The total ram mechanism interaction forces between the booster and orbiter are a function of the forces produced by activation of the mechanisms and the forces because of structural deflection of each mechanism.

The force magnitude produced by the activation of each ram mechanism was assumed to have a predetermined time history as illustrated in figure 8. The force equation of each ram is

$$FRAM = FRM\left(1 - e^{-\lambda t}\right) \tag{57}$$

where FRM is the maximum ram force and λ is a positive constant. The force vector from the above ram force magnitude is calculated by multiplying this magnitude times a unit vector along the line of action of the ram. The orientation of each ram is calculated in the same manner as the link members. The loop equations that define the ram attach point on the orbiter relative to the booster c.g. can be equated. Therefore, for ram mechanism 1 (forward mechanism)

$$\overrightarrow{PBSR}_1 + \overrightarrow{SBD}_{R1} + \overrightarrow{SRM}_1 = \overrightarrow{SBO} + \overrightarrow{POSR}_1 + \overrightarrow{SOD}_{R1} \tag{58}$$

Equation (58) can be solved for the vector $\overrightarrow{SRM}_1$, which defines the line of action of the ram force. Thus,

$$\overrightarrow{SRM}_1 = \overrightarrow{SBO} + \overrightarrow{POSR}_1 + \overrightarrow{SOD}_{R1} - \overrightarrow{PBSR}_1 - \overrightarrow{SBD}_{R1} \tag{59}$$

The forces on the booster and orbiter because of activation of ram 1 are

$$\overrightarrow{BRMV}_1 = -FRAM \cdot \overrightarrow{SRM}_1 \Big/ \left|\overrightarrow{SRM}_1\right| \tag{60}$$

and

$$\overrightarrow{ORMV}_1 = FRAM \cdot \overrightarrow{SRM}_1 \Big/ \left|\overrightarrow{SRM}_1\right| \tag{61}$$

The corresponding torques on each vehicle are

$$\overrightarrow{TBRM}_1 = \left(\overrightarrow{PBSR}_1 + \overrightarrow{SBD}_{R1}\right) \times \overrightarrow{BRMV}_1 \tag{62}$$

and

$$\overrightarrow{TORM}_1 = \left(\overrightarrow{POSR}_1 + \overrightarrow{SOD}_{R1}\right) \times \overrightarrow{ORMV}_1 \tag{63}$$

The structural forces produced by the ram mechanisms are a function of the ram stiffness characteristics and the structural displacements of the mechanisms. As previously mentioned, the ends of the ram mechanisms are pinned parallel to the Y-axis of the booster and attached as a ball joint on the orbiter. The lateral (YB-direction) displacements of the orbiter ram attach point relative to its booster attach point are calculated from equation (59), that is,

$$DLY_{R1} = SRMY_1 - SYI_1 \tag{64}$$

where SYI_1 is the unstroked length of ram 1.

This deflection is multiplied by the lateral stiffness of the ram mechanism to yield the lateral force at the orbiter attach point.

$$FRY_1 = -KRL_1 \cdot DLY_{R1} \tag{65}$$

The reaction force at the booster attach point is simply

$$FRBY_1 = -FRY_1 \tag{66}$$

The corresponding torque at the booster attach point because of the lateral deflection force is

$$TRB_1 = \left|\overrightarrow{SRM}_1\right| \cdot FRY_1 \tag{67}$$

Because of ram deflection, the lateral force acts along the YB-axis, and the torque acts about the XB-axis (fig. 1). Thus, the force and torque vectors caused by ram mechanism deflections are

$$\overrightarrow{FRB}_1 = FRBY_1 \bar{j}_B \tag{68}$$

and

$$\overrightarrow{TRB}_1 = TRB_1 \bar{i}_B \tag{69}$$

Because of ram deflections, the force vector on the orbiter is calculated by transferring FRY_1 from the booster to orbiter coordinate system. Thus, from equations (1) and (3), the force on the orbiter because of ram deflection is given by equation (70) below.

$$\begin{Bmatrix} FROX_1 \\ FROY_1 \\ FROZ_1 \end{Bmatrix} = \begin{bmatrix} \\ GIO(I,J) \\ \\ \end{bmatrix} \begin{bmatrix} \\ GIB(I,J) \\ \\ \end{bmatrix}^T \begin{Bmatrix} 0 \\ FRY_1 \\ 0 \end{Bmatrix} \tag{70}$$

The forces from ram mechanism 2 (rear mechanism) are calculated in the same manner as for ram mechanism 1.

The total ram mechanism forces acting on the booster and orbiter are

$$\overrightarrow{BRMV} = \overrightarrow{BRMV}_1 + \overrightarrow{BRMV}_2 + \overrightarrow{FRB}_1 + \overrightarrow{FRB}_2 \tag{71}$$

and

$$\overrightarrow{ORMV} = \overrightarrow{ORMV}_1 + \overrightarrow{ORMV}_2 + \overrightarrow{FRO}_1 + \overrightarrow{FRO}_2 \tag{72}$$

The corresponding torques are

$$\overrightarrow{TBRM} = \overrightarrow{TBRM}_1 + \overrightarrow{TBRM}_2 + \overrightarrow{TRB}_1 + \overrightarrow{TRB}_2 + \left(\overrightarrow{PBSR}_1 + \overrightarrow{SBD}_{R1}\right) \times \overrightarrow{FRB}_1 + \left(\overrightarrow{PBSR}_2 + \overrightarrow{SBD}_{R2}\right) \times \overrightarrow{FRB}_2 \tag{73}$$

and

$$\overrightarrow{TORM} = \overrightarrow{TORM}_1 + \overrightarrow{TORM}_2 + \left(\overrightarrow{POSR}_1 + \overrightarrow{SOD}_{R1}\right) \times \overrightarrow{FRO}_1 + \left(\overrightarrow{POSR}_2 + \overrightarrow{SOD}_{R2}\right) \times \overrightarrow{FRO}_2 \tag{74}$$

THRUST FORCES

The thrust vector from each engine on the booster and orbiter was calculated from the thrust magnitude and from the engine gimbal angles. The thrust magnitude on both the booster and orbiter was scheduled to achieve desired thrust-to-weight ratios. The thrust scheduling of each vehicle is given in figure 2. The engine gimbal angles are calculated from the TVC logic, which is presented for planar rotations in reference 5 and is extended to cover full vehicle rotations.

The TVC logic is described for the booster engines as follows. The booster attitude deviations from the commanded (desired) attitude about each axis are

$$\begin{aligned} DTB1 &= \psi B - \psi BC \\ DTB2 &= \theta B - \theta BC \\ DTB3 &= \phi B - \phi BC \end{aligned} \tag{75}$$

These attitude deviations are transferred into the booster coordinate system so that they can be combined with the booster angular velocity components to calculate the booster error signals. The attitude deviations are calculated by differencing Euler angles. These deviations are small; thus, they are assumed to be vector quantities. The deviations are transferred into the booster system using the inverse of equation (6). The attitude deviations expressed in the booster coordinate system are

$$\begin{Bmatrix} ETBX \\ ETBY \\ ETBZ \end{Bmatrix} = \begin{bmatrix} -SIN\theta B & 0 & 1 \\ COS\theta B \cdot SIN\phi B & COS\phi B & 0 \\ COS\theta B \cdot COS\phi B & SIN\phi B & 0 \end{bmatrix} \begin{Bmatrix} DTB1 \\ DTB2 \\ DTB3 \end{Bmatrix} \tag{76}$$

The error signals of the booster are calculated as a weighted sum of the attitude deviation and the angular velocity components. The weighting factors are called gains, and they reflect the desired weighting of the component by which they are multiplied. Therefore,

$$\begin{aligned} EBX &= ETBX + RX \cdot \omega BX \\ EBY &= ETBY + RY \cdot \omega BY \\ EBZ &= ETBZ + RZ \cdot \omega BZ \end{aligned} \tag{77}$$

These error signals are integrated to yield the error integrals, that is,

$$\begin{Bmatrix} EBXI \\ EBYI \\ EBZI \end{Bmatrix} = \int \begin{Bmatrix} EBX \\ EBY \\ EBZ \end{Bmatrix} dt + \begin{Bmatrix} EBXI_I \\ EBYI_I \\ EBZI_I \end{Bmatrix} \tag{78}$$

The gimbal angles and rates of each booster engine required to correct the booster attitude deviations are calculated from the error signals and error integrals. The gimbal angle commands for the jth booster engine are calculated as a weighted sum of the error signals and the error integrals, that is,

$$\begin{aligned} GBCX_j &= DX_{Bj}\left(EBX + XI_{Bj} \cdot EBXI\right) \\ GBCY_j &= DY_{Bj}\left(EBY + YI_{Bj} \cdot EBYI\right) \\ GBCZ_j &= DZ_{Bj}\left(EBZ + ZI_{Bj} \cdot EBZI\right) \end{aligned} \tag{79}$$

Because the engine cannot move instantaneously to this commanded angle, the gimbal rate command is calculated. These commands for the jth engine are

$$\begin{aligned} GBXD_j &= CX_{Bj}\left(GBCX_j - \phi BE_j\right) \\ GBYD_j &= CY_{Bj}\left(GBCY_j - \theta BE_j\right) \\ GBZD_j &= CZ_{Bj}\left(GBCZ_j - \psi BE_j\right) \end{aligned} \tag{80}$$

The gimbal rates are limited by the physical size of the engine and the mechanism that gimbals the engine. The gimbal angles of the jth engine can be calculated from the gimbal rates and the initial gimbal angles, that is,

$$\begin{Bmatrix} \phi BE \\ \theta BE \\ \psi BE \end{Bmatrix}_j = \int \begin{Bmatrix} GBXD \\ GBYD \\ GBZD \end{Bmatrix}_j dt + \begin{Bmatrix} \phi BE_I \\ \theta BE_I \\ \psi BE_I \end{Bmatrix}_j \tag{81}$$

The engine roll angle ϕBE_j can be combined with engine pitch or yaw angles to produce roll control. For the case of two side-by-side engines, the roll angles can be combined with the pitch angles for the roll control, that is,

$$\begin{aligned} \theta BE_1' &= \theta BE_1 + KRR_1 \cdot \phi BE_1 \\ \theta BE_2' &= \theta BE_2 - KRR_2 \cdot \phi BE_2 \end{aligned} \tag{82}$$

These equations represent one engine pitching up while the other pitches down to create the desired roll torque.

Thus, the gimbal angles of each engine are known, and, assuming the engine thrust acts along the centerline of the engine, the engine thrust vector can be calculated, that is,

$$\begin{Bmatrix} THRVBX \\ THRVBY \\ THRVBZ \end{Bmatrix}_j = \begin{bmatrix} GBE(I,J) \end{bmatrix} \begin{Bmatrix} TMAGB \\ O \\ O \end{Bmatrix}_j \tag{83}$$

The engine gimbal angles of the orbiter are calculated in the same manner as those of the booster; thus, the orbiter thrust vector is

$$\begin{Bmatrix} THRVOX \\ THRVOY \\ THRVOZ \end{Bmatrix}_j = \begin{bmatrix} GOE(I,J) \end{bmatrix} \begin{Bmatrix} TMAGO \\ O \\ O \end{Bmatrix}_j \tag{84}$$

The total booster and orbiter thrust are

$$\overrightarrow{THRVB} = \sum_{j=1}^{M1} \overrightarrow{THRVB}_j \tag{85}$$

and

$$\overrightarrow{THRVO} = \sum_{j=1}^{M2} \overrightarrow{THRVO}_j \tag{86}$$

The corresponding c.g. torques are

$$\overrightarrow{THMB} = \sum_{j=1}^{M1} \left(\overrightarrow{VEB}_j \times \overrightarrow{THRVB}_j \right) \tag{87}$$

and

$$\overrightarrow{THMO} = \sum_{j=1}^{M2} \left(\overrightarrow{VEO}_j \times \overrightarrow{THRVO}_j \right) \tag{88}$$

STRUCTURAL DYNAMICS

The structural response of each vehicle can be calculated from the external loading and the modal characteristics of that vehicle. The external loads on each vehicle are the link forces, ram forces, and thrust forces. The modal characteristics of each vehicle are calculated from their respective structural models. The modes and frequencies of a multidegree-of-freedom model of both booster and orbiter can be developed as described in reference 6.

For this mathematical model, the structural response of the vehicles is included to examine its effect on the interaction link forces between vehicles. Because the forces generated in each link member are a function of the position and orientation of the link end points, the structural response of each vehicle at the link attach points is of interest.

The structural displacement at the link attach points can be related to the structural response of each vehicle by the following equations.

$$\{SBD\} = [\Phi B]\{\xi B\} \tag{89}$$

$$\{SOD\} = [\Phi O]\{\xi O\} \tag{90}$$

where $[\phi B]$ and $[\phi O]$ are the "free-free" modal matrices of the booster and orbiter, ξB and ξO are the generalized displacements, and SBD and SOD are the structural displacements at specific points of interest.

The generalized displacements are calculated in the following manner. The generalized acceleration of the booster as developed in reference 6 can be written as

$$\{\ddot{\xi}B\} = \left[MBG\right]^{-1}[\Phi B]^{T}\{FBE\} - 2\zeta\left[BMG\right]\{\dot{\xi}B\} - \left[BMG^{2}\right]\{\xi B\} \tag{91}$$

where [MBG] is the generalized mass matrix and [BMG] are the natural frequencies for the booster structural model. The constant ζ represents the percent of critical damping, and {FBE} is the vector of external forces acting on the booster. The generalized acceleration of the orbiter is of the same form as equation (91).

The generalized accelerations of each vehicle can be integrated to yield the corresponding generalized velocities and displacements, that is,

$$\begin{aligned}\{\dot{\xi}B\} &= \int\{\ddot{\xi}B\}dt + \left\{\dot{\xi}B_{I}\right\} \\ \{\dot{\xi}O\} &= \int\{\ddot{\xi}O\}dt + \left\{\dot{\xi}O_{I}\right\}\end{aligned} \tag{92}$$

and

$$\begin{aligned}\{\xi B\} &= \int\{\dot{\xi}B\}dt + \left\{\xi B_{I}\right\} \\ \{\xi O\} &= \int\{\dot{\xi}O\}dt + \left\{\xi O_{I}\right\}\end{aligned} \tag{93}$$

The generalized displacements of equation (93) can be used in equations (89) and (90) to yield structural displacements of each vehicle at the desired node points (fig. 9).

COMPUTATIONS

As noted in the introduction, the mathematical model is incorporated into a computer program so that the staging maneuver can be simulated. The computer program is described in appendix B. The primary input parameters used in the staging simulations are divided into two categories: those that were fixed for all simulations and those that were varied between simulations.

Fixed Input Data

The masses, inertias, and c.g. locations of each vehicle are given in table I. These quantities were assumed to be fixed with respect to each vehicle over the duration of the separation maneuver. The inertial coordinate system was positioned at the initial booster c.g. location, and the c.g. of the orbiter is defined relative to this initial position.

The position vectors of the link and ram mechanism attach points relative to the c. g. of each vehicle are given in table II. Also, the position vectors of the booster and and orbiter engines relative to their respective centers of gravity are presented in table II. For the simulations presented in this report, the booster and orbiter were each assumed to have one engine with equivalent thrust of the multiple engines of the respective vehicles described in reference 1. The TVC gains for each vehicle are given in table III. The booster engine TVC logic was used during the swing phase, but the orbiter engine gimbal angles were constant over this period.

The vehicle structural data used in the simulations were very limited. Only limited data were available because of the preliminary stage of development of the Space Shuttle Program. The numbering of the orbiter node points is illustrated in figure 9, and the corresponding modal matrix for the orbiter is given in table IV. The orbiter natural frequencies and generalized masses also are given in table IV. No booster structural data were used because no data were known to exist for the configuration being simulated.

Variable Input Data

Certain quantities were varied between simulations so that the effects of these variations could be examined. These quantities include vehicle thrust scheduling, ram forcing function, and link elastic properties.

Case 1 of the simulations represented the nominal case for the link-ram system. The variable input data, coupled with the fixed input data, represent the baseline input for the nominal separation sequence. The subsequent cases are simulated with perturbations in the variable input data of case 1. The thrust scheduling for case 1 is presented in figure 2, and the ram forcing function for this case is presented in figure 8. The link stiffness characteristics for this system are given in table V. No elastic modes were used in cases 1 to 4.

Case 2 was simulated with a 100-percent increase in the stiffness of each link member.

Case 3 was simulated with different ram mechanism force characteristics. The ram force was simulated as a step function ($\lambda = \infty$) and for a lower than nominal onset rate ($\lambda = 8$) as shown in figure 8.

Case 4 was simulated with the orbiter at full thrust at the beginning of the swing phase, as opposed to approximately 67 percent of full thrust in the nominal case.

Case 5 represented the nominal separation sequence with the first orbiter mode included and the nominal separation sequence with the first 10 orbiter modes included. These modes correspond to the lowest natural frequency of the orbiter.

RESULTS

Results are presented for the five cases of the separation maneuver that were simulated. The parameters that are presented include swing-link loads, swing-link rotation angle, booster and orbiter angular velocities, relative c.g. translational velocities, and booster engine gimbal angle.

The load time histories in the forward and rear swing links for case 1 are presented in figures 10 and 11. The loads in the forward swing links (fig. 10) oscillate between compression and tension during the swing phase of the staging sequence. The loads in the rear swing links (fig. 11) remain primarily in tension during the swing phase. Tension loads in both the forward and aft links produce negative torques on the booster c.g. because the attach points of these links are forward of the booster c.g. (table II). Tension loads in the forward and aft links also produce negative torques on the orbiter because of the position and orientation of the links relative to the orbiter c.g. (table II).

The angular velocities about the Y-axis of each vehicle for case 1 are presented in figures 12 and 13. The X- and Z-components of angular velocity were zero in all cases simulated. In all cases, both the booster and orbiter build up a negative (nose down) angular velocity during the swing phase. The booster engine gimbal angle is presented in figure 14. This gimbal angle is decreasing throughout the swing phase because the booster engine is trying to correct the negative booster angular velocity. The swing angles of both the forward and rear swing links are approximately equal. The forward link-swing angle (fig. 15) is plotted relative to its initial angle, which is 17.7°. The engine gimbal angle and the link-swing angle are shown only for case 1 because only small changes in these values existed in the subsequent cases.

The relative axial (XI-direction) and normal (ZI-direction) velocities between the booster and orbiter centers of gravity are presented in figures 16 and 17, respectively. These linear velocities, coupled with the angular velocities, can be used to calculate the relative velocity between any points on the booster and orbiter.

The effects of increased link stiffness on the staging dynamics were examined in case 2. The forward and rear swing-link loads are presented in figures 18 and 19. The frequency of oscillation in both the forward and rear swing-link loads is about 25 percent higher than nominal. The higher frequencies would be expected for the increased link stiffnesses. The maximum value of the forward link loads (fig. 18) are about the same as nominal, but the peak tension loads in the rear swing links (fig. 19) are about 15 percent higher than nominal. The angular velocities for this case are presented in figures 20 and 21. The booster angular velocity (fig. 20) is about the same as the nominal case, but the orbiter angular velocity (fig. 21) is more oscillatory, and its peak value is about 10 percent lower than nominal. The relative translational velocities of this case are presented in figures 22 and 23. These values are virtually unchanged from the nominal case. Thus, the increased link stiffness does significantly change the relative motion between the booster and orbiter during the separation maneuver.

Case 3 was simulated to examine the effects of different ram mechanism forces on the separation performance. The step input ram force ($\lambda = \infty$) represented about a 20-percent increase in impulse; the lower onset ram force ($\lambda = 8$) represented a

30-percent decrease in impulse. The loads in the forward and rear swing links for this case are presented in figures 24 and 25. The forward link loads (fig. 24) for the step ram force are approximately 35 percent higher than nominal in compression; the rear link loads (fig. 25) for this ram force were about 35 percent higher than nominal in tension. The maximum loads in both the forward and rear links for the lower onset ram force are about the same as nominal. The booster and orbiter angular velocities for this case (figs. 26 and 27) build up negative values faster for the step ram force than for the lower onset ram force. However, the booster angular velocities (fig. 26) at the time of release (Tsep) are approximately equal for both ram forces and are approximately 5 percent below nominal. Also, the orbiter angular velocities (fig. 27) at release are approximately equal for both ram forces and are approximately 10 percent below nominal. The relative axial velocity (fig. 28) for the step ram force is about 15 percent higher than nominal and about 10 percent below nominal for the lower onset ram force at release. Similarly, the relative normal velocity (fig. 29) for the step ram force is about 10 percent higher than nominal, and it is 10 percent below nominal for the lower onset ram force. Thus, the relative motion of the booster and orbiter is proportional to the total impulse of the ram-mechanism forces. However, this proportionality is not one to one because the thrust forces also contribute to the total impulse on each vehicle.

Case 4 was run with higher than nominal orbiter thrust at the beginning of the swing phase (Tswing). This higher orbiter thrust level represented a 30-percent increase in impulse to orbiter during the swing phase. The forward link load time history for this case (fig. 30) has peak tension and compression loads that are about the same as nominal. Likewise, the maximum values of the rear link loads (fig. 31) are about equal to nominal. The booster and orbiter angular velocities (figs. 32 and 33) are each about 12 percent higher than nominal at release. The relative axial velocity for this case (fig. 34) is approximately 20 percent higher than nominal at release, and the relative normal velocity (fig. 35) is approximately 5 percent higher than nominal at release. Thus, the increased orbiter thrust in this case represents an increase in impulse acting axially on the orbiter, and this increase is reflected in the larger relative axial velocity.

The effects of the orbiter modal data on the separation performance are examined in case 5. The forward swing-link loads (fig. 36) for one mode and those for 10 modes are similar in magnitude but slightly different in frequency. The maximum tension and compression values of these loads are about 15 percent below nominal. The rear link loads (fig. 37) for one mode and those for 10 modes are also similar in magnitude and slightly different in frequency. The magnitude of these loads is about equal to nominal although the maximum tension load for 10 modes is about 8 percent higher than nominal. The booster angular velocities are presented in figure 38 and are about the same as nominal for one mode and for 10 modes. The orbiter angular velocities (fig. 39) are about 15 percent below nominal at release for both one mode and 10 modes. The relative axial and normal velocities for this case (figs. 40 and 41) are virtually unchanged from nominal for both one mode and 10 modes. Thus, including the orbiter structural response does not significantly change the relative motion of the booster and orbiter during the separation maneuver.

The linear and angular velocities of the booster and orbiter were used to calculate the separation distance between points on each vehicle during the separation maneuver.

The separation distance at the various points was used as a check for possible recontact between the vehicles. In all simulated cases, no recontact between the booster and orbiter occurred.

The stresses resulting from both the tension and compression loads in the swing link members were well below the proportional limit stress of these members for all cases simulated.

CONCLUSIONS

The foregoing discussion of the staging dynamics of a space shuttle configuration using a link-ram staging mechanism leads to the following conclusions.

1. For all cases simulated, the translational and rotational motion of the booster and orbiter during the separation maneuver is sufficient to ensure no recontact between the vehicles.

2. The loads generated in the swing-link members during the swing phase of the staging sequence produce stresses that are well below the proportional limit stress of these members.

3. Variations in the stiffnesses of the swing-link members change the maximum loads in these members but do not significantly change the relative motion of the vehicle during the staging maneuver.

4. Variations in the total impulse from the orbiter thrust and from the ram mechanism forcing function produce appreciable change in the relative motion of the booster and orbiter during the staging maneuver.

5. Including the orbiter structural response in the staging simulations produces only a small deviation in the link loads and a negligible change in the relative motion of the vehicles.

The following recommendations are made concerning the further analysis of the staging maneuver.

1. Booster heating caused by orbiter engine plume impingement should be evaluated.

2. The effects of plume impingement forces on the staging dynamics should be examined.

3. The nonsymmetric loading on each vehicle because of deviations in link release times should be examined.

4. The effects of fuel slosh on the staging dynamics should be evaluated.

5. The performance of the link-ram staging system under high aerodynamic load conditions should be evaluated.

Manned Spacecraft Center
National Aeronautics and Space Administration
Houston, Texas, October 11, 1972
986-15-31-06-72

REFERENCES

1. Anon.: Phase B Final Report. Vol. II, Technical Summary, Book 3, Booster Vehicle Definition, Space Div. of N. Am. Rockwell Corp., June 1971.

2. Thomson, W. T.: Introduction to Space Dynamics. John Wiley and Sons, Inc., 1961.

3. Zupp, George A.; and Doiron, Harold H.: A Mathematical Procedure for Predicting the Touchdown Dynamics of a Soft-Landing Vehicle. NASA TN D-7045, 1971.

4. Przemieniecki, J. S.: Theory of Matrix Structural Analysis. McGraw-Hill Book Co., Inc., 1968.

5. Carrie, G. W.; and Hurley, M. J.: Space Shuttle Separation System Analysis, A Capability Assessment. Convair Aerospace Div. of General Dynamics, Rep. 76-549-4-172, June 1971.

6. Meirovitch, L.: Analytical Methods in Vibrations. Macmillan Co., 1967.

TABLE I. - VEHICLE MASS PROPERTIES

Parameter	Value
Mass, kg	
MBT	365 234
MOT	368 823
Inertias, kg-m^2	
IXXB	13 146 049
IYYB	178 019 415
IZZB	180 188 730
IXYB	0
IXZB	3 511 579
IYZB	0
IXXO	6 986 550
IYYO	43 962 525
IZZO	49 122 783
IXYO	0
IXZO	695 537
IYZO	0
Center of gravity, m	
SBX	0
SBY	0
SBZ	0
SOX	23. 056
SOY	0
SOZ	10. 300

TABLE II. - LINK, RAM, AND ENGINE LOCATION

Vector	Axis			Vector	Axis		
	X	Y	Z		X	Y	Z
Link attach points, m							
$POSB_1$	30.68	-1.777	-6.65	$POSO_1$	3.03	-1.777	2.17
$POSB_2$	30.68	-1.777	-6.65	$POSO_2$	3.03	-1.777	2.17
$POSB_3$	26.11	-1.777	-6.65	$POSO_3$	3.03	-1.777	2.17
$POSB_4$	26.11	-1.777	-6.65	$POSO_4$	3.03	-1.777	2.17
$POSB_5$	10.26	-1.777	-6.65	$POSO_5$	-17.39	-1.777	2.17
$POSB_6$	10.26	-1.777	-6.65	$POSO_6$	-17.39	-1.777	2.17
$POSB_7$	5.69	-1.777	-6.65	$POSO_7$	-17.39	-1.777	2.17
$POSB_8$	5.69	-1.777	-6.65	$POSO_8$	-17.39	-1.777	2.17
Ram mechanism attach points, m							
$PBSR_1$	30.68	0	-6.65	$POSR_1$	3.03	0	2.17
$PBSR_2$	5.69	0	-6.65	$POSR_2$	-17.39	0	2.17
Engine gimbal points, m							
BEV	-21.56	0	-1.77	OEV	-15.26	0	-.648

TABLE III. - THRUST VECTOR CONTROL GAINS

Gain	Vehicle	
	Booster	Orbiter
RX	0.7	2
RY	.7	2
RZ	.7	2
DX	2	2
DY	2	2
DZ	2	2
XI	.1	.05
YI	.1	.05
ZI	.1	.05
CX	15	15
CY	15	15
CZ	15	15

TABLE IV. - ORBITER MODAL MATRIX, NATURAL FREQUENCIES, AND GENERALIZED MASSES

Node	Mode									
	1	2	3	4	5	6	7	8	9	10
1X	0.00907	-0.00340	0.06036	-0.04472	0.07836	-0.13010	-0.13955	-0.81576	0.65862	0.17119
1Z	-.70784	-.97249	.00272	.00894	.21479	-.46816	.06518	.07037	.10938	.01714
2X	.00907	-.00340	.06036	-.04472	.07836	-.13010	-.13955	-.81576	.65862	.17119
2Z	-.70784	-.97249	.00272	.00894	.21479	-.46816	.06518	.07037	.10938	.01714
3Z	.99642	-.46076	.11946	-.04861	-.85350	-.71552	-.73947	.19871	-.13052	-.02099
4Z	.99642	-.46076	.11946	-.04861	-.85350	-.71552	-.73947	.19871	-.13052	-.02099
5X	-.14138	.12760	-.08165	-.02682	.09469	-.05436	.20714	.34208	-.33816	-.02914
5Z	1.3894	-.86968	.33203	-.05869	-1.1818	-1.0365	-2.1068	.50503	-.27140	.27498
6X	.00907	-.00340	.06036	-.04472	.07836	-.13010	-.13955	-.81576	.65862	.17119
6Z	-.70784	-.97249	.00272	.00894	.21479	-.46816	.06518	.07037	.10938	.01714
7Z	.99642	-.46076	.11946	-.04861	-.85350	-.71552	-.73947	.19871	-.13052	-.02099

Notes:
(1) $\omega_1 = 2.8697$
(2) $\omega_2 = 4.8610$
(3) $\omega_3 = 6.8383$
(4) $\omega_4 = 7.5418$
(5) $\omega_5 = 7.9059$
(6) $\omega_6 = 8.0210$
(7) $\omega_7 = 10.5549$
(8) $\omega_8 = 11.7859$
(9) $\omega_9 = 11.9221$
(10) $\omega_{10} = 12.9829$
(11) $MOG_i = 173227.3$
(12) i = 1, 10

Dimensions:
(1) MODAL MATRIX = m/m
(2) ω = Hz
(3) MOG = kg

TABLE V. - LINK STIFFNESS CHARACTERISTICS

[$E = 1.1 \times 10^{11}$ N/m^2; $G = 4.068 \times 10^{10}$ N/m^2; proportional limit stress = 8.55×10^{8} N/m^2]

Link	Properties			
	ℓ, m	A, m^2	I, m^4	J, m^4
1	4.829	0.0110	0.00018	0.00036
2	4.829	.0110	.00018	.00036
3	1.473	.0039	.0035	.0069
4	1.473	.0039	.0035	.0069
5	4.829	.0064	.000035	.000071
6	4.829	.0064	.000035	.000071
7	1.473	.0039	.0035	.00070
8	1.473	.0039	.0035	.00070

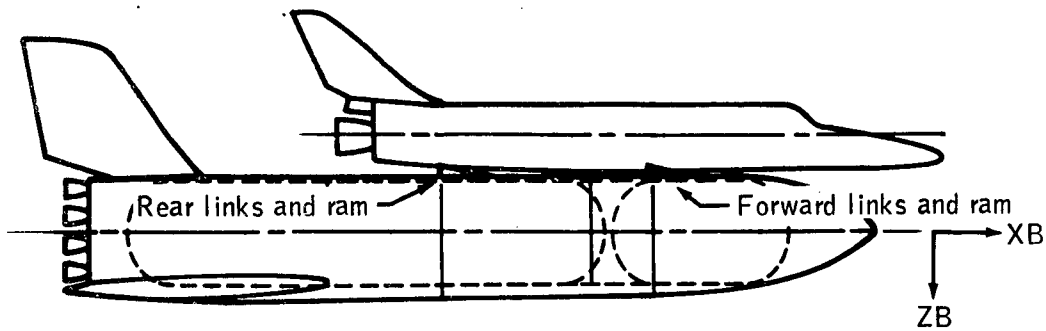

(a) Launch configuration and section locations.

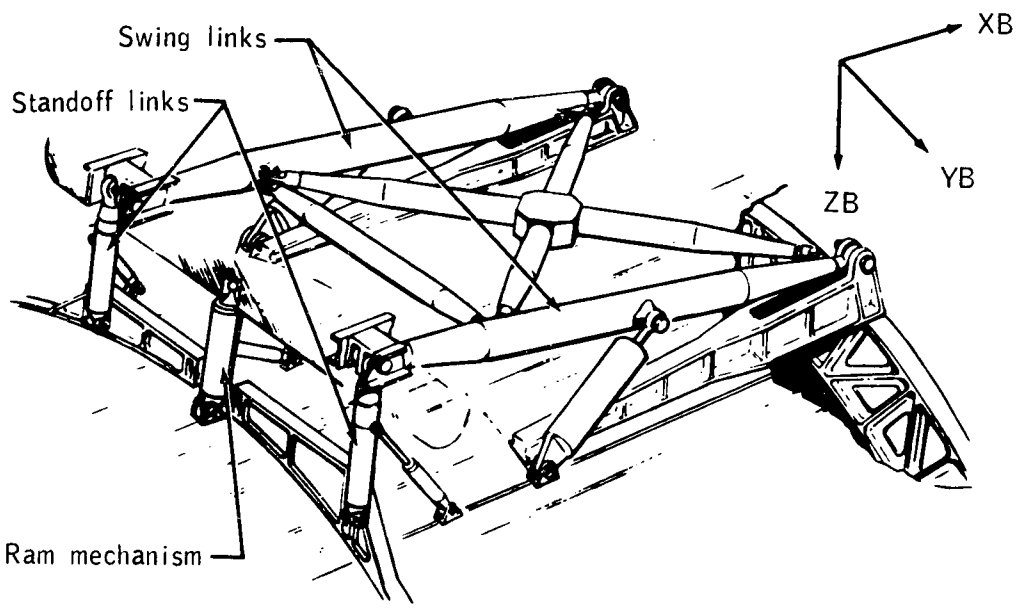

(b) Forward or rear link-ram section.

Figure 1. - Illustration of separation system.

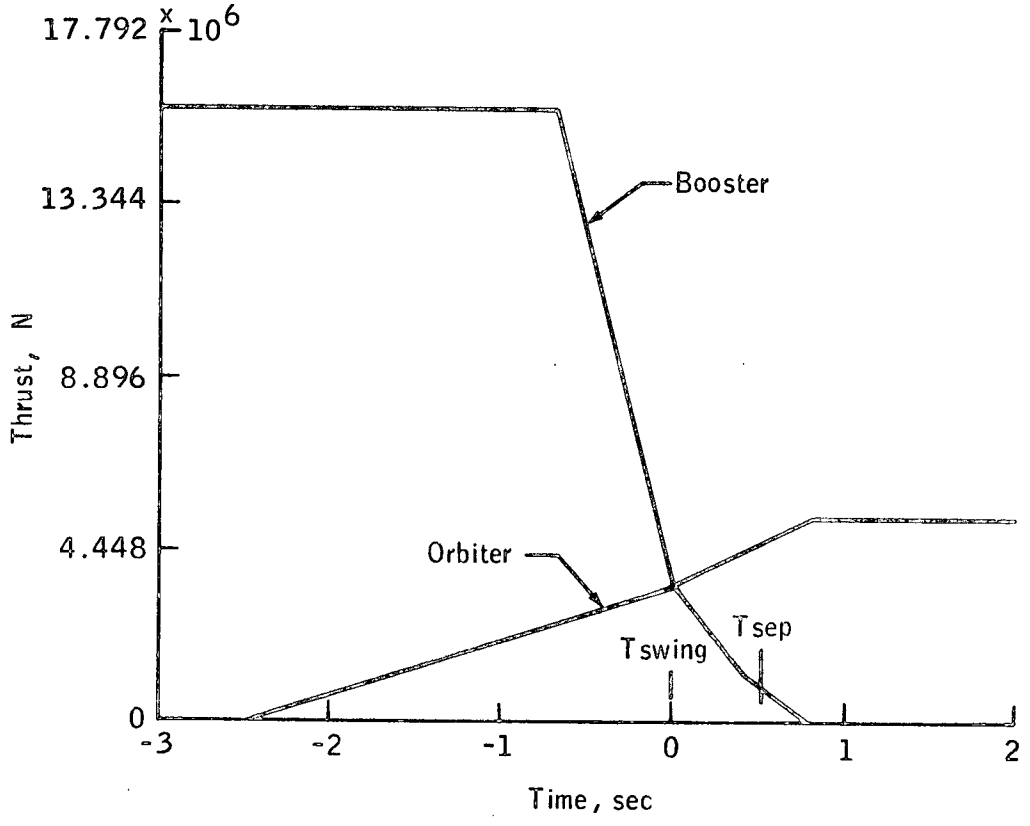

Figure 2.- Booster and orbiter thrust scheduling.

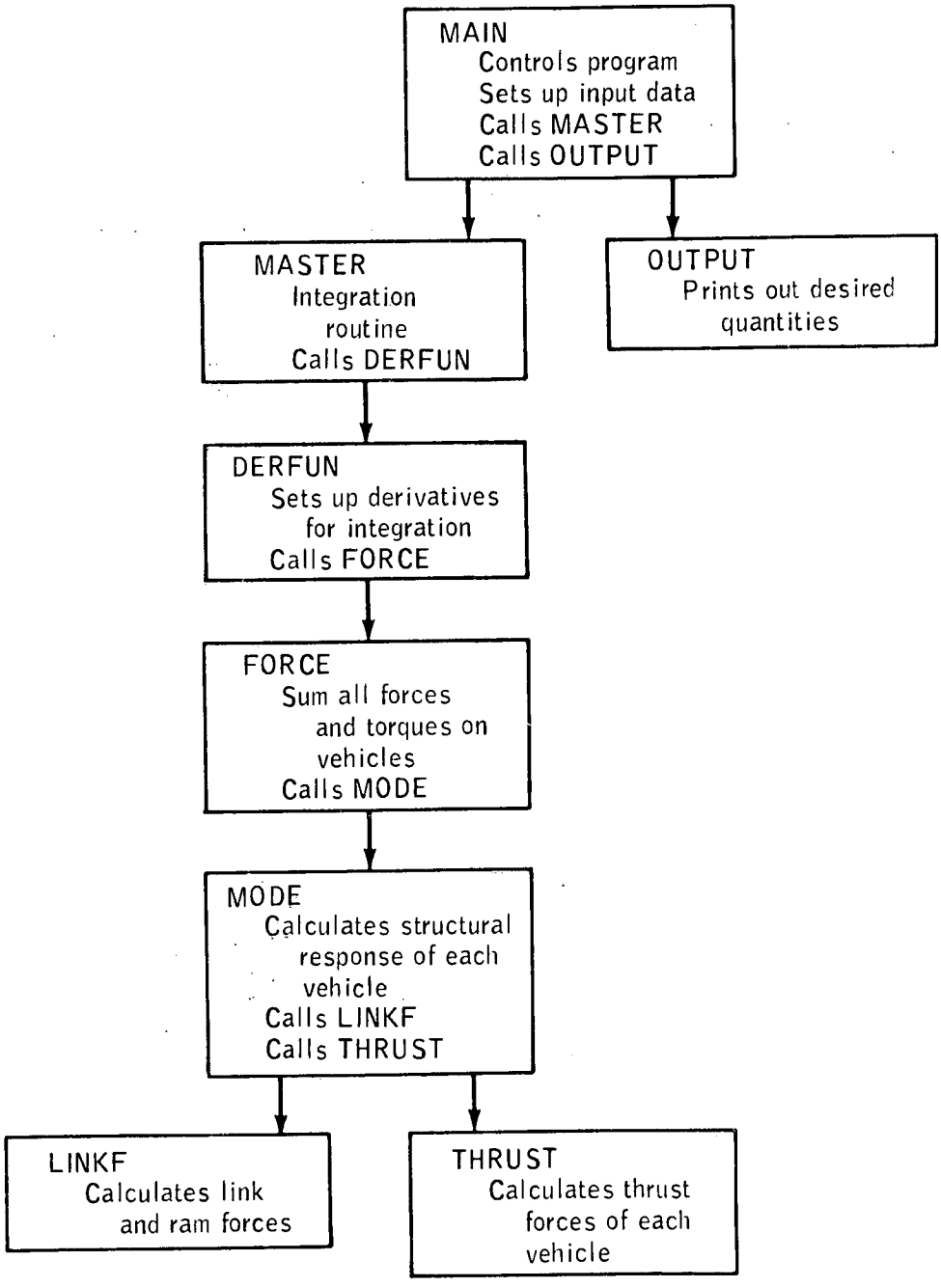

Figure 3.- Computer program flow chart.

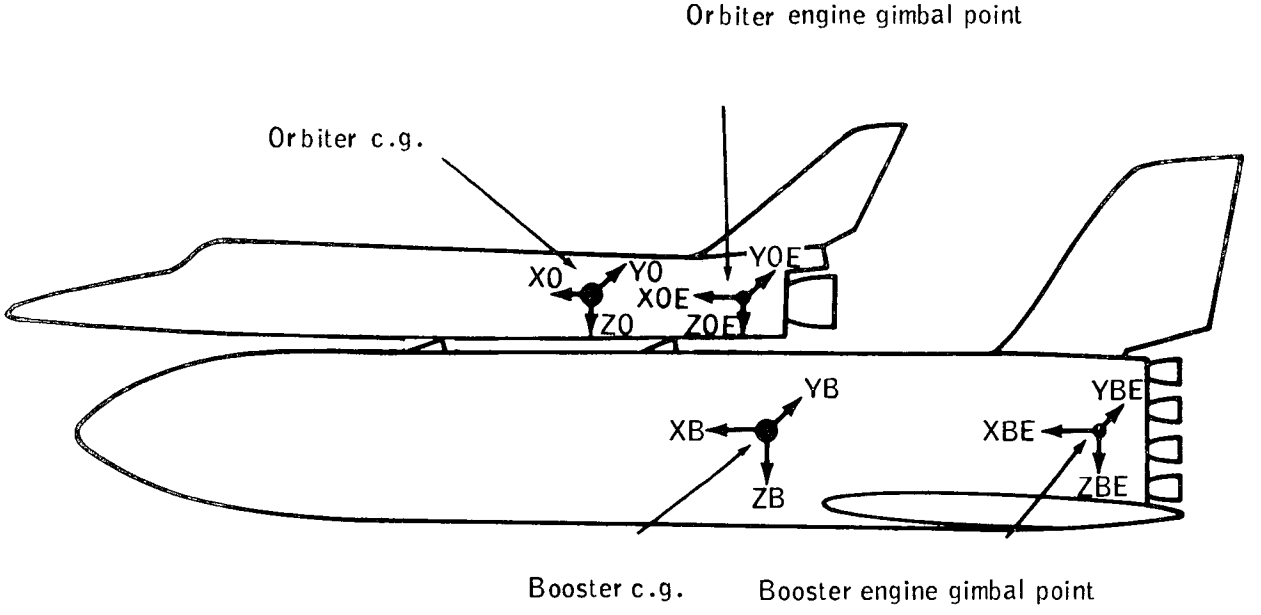

Figure 4.- Illustration of coordinate systems.

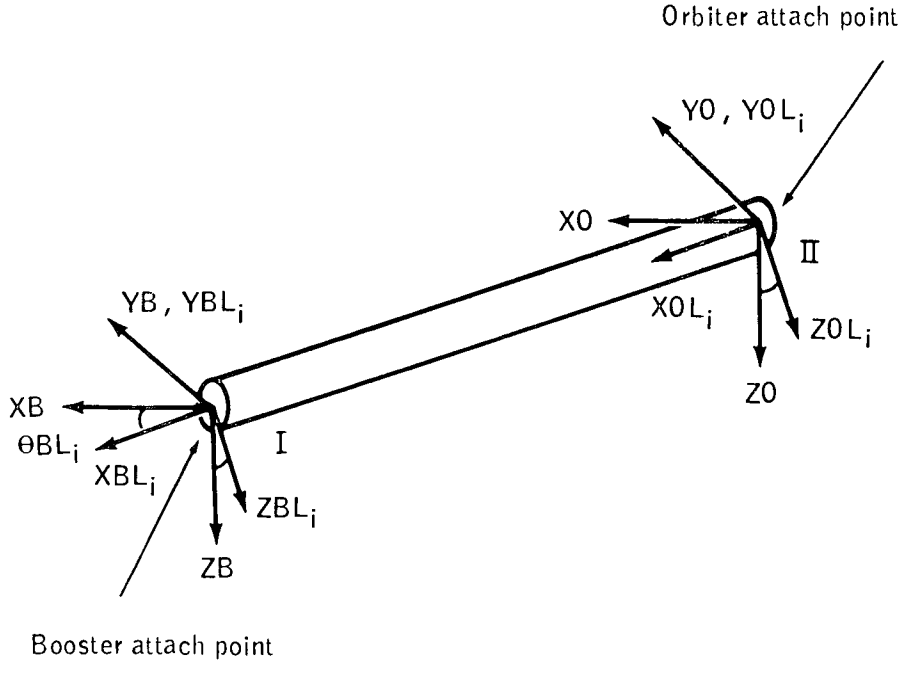

Figure 5.- Link element coordinate systems.

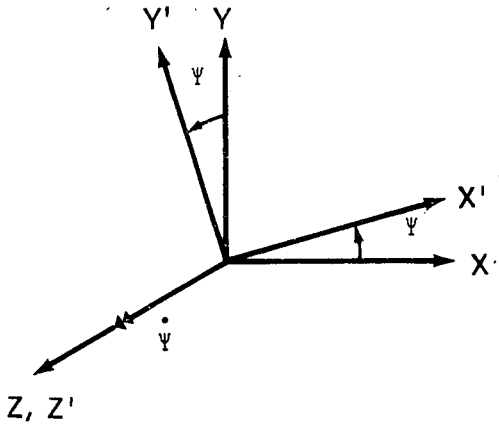

(a) The ψ rotation of XY-plane about Z-axis.

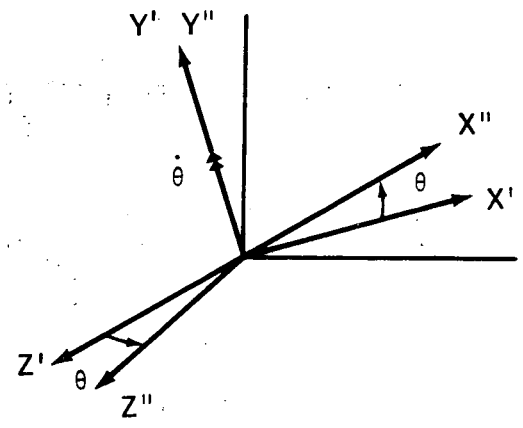

(b) The θ rotation of X'Z'-plane about Y'-axis.

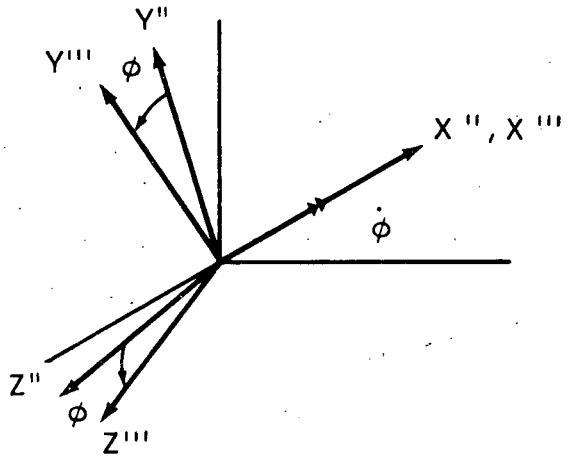

(c) The ϕ rotation of Y"Z"-plane about X"-axis.

Figure 6.- Euler angle rotations.

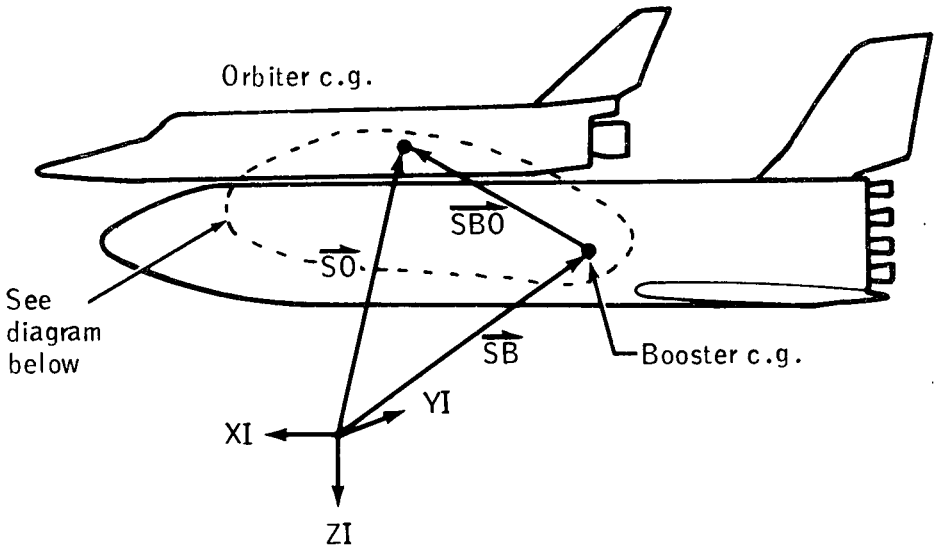

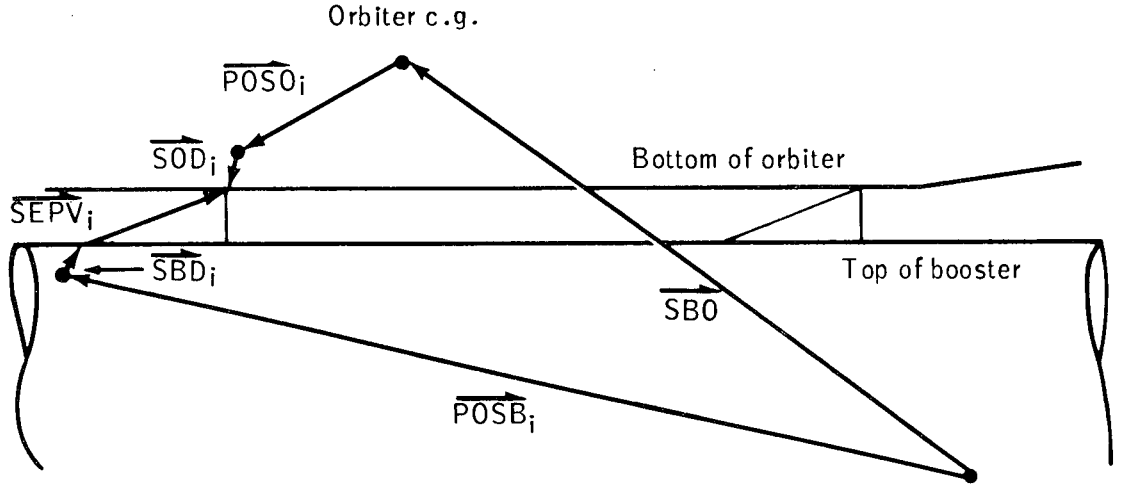

$$\overrightarrow{POSB_i} + \overrightarrow{SBD_i} + \overrightarrow{SEPV_i} = \overrightarrow{SBO} + \overrightarrow{POSO_i} + \overrightarrow{SOD_i}$$

Figure 7. - Vector diagram for link position calculations

E

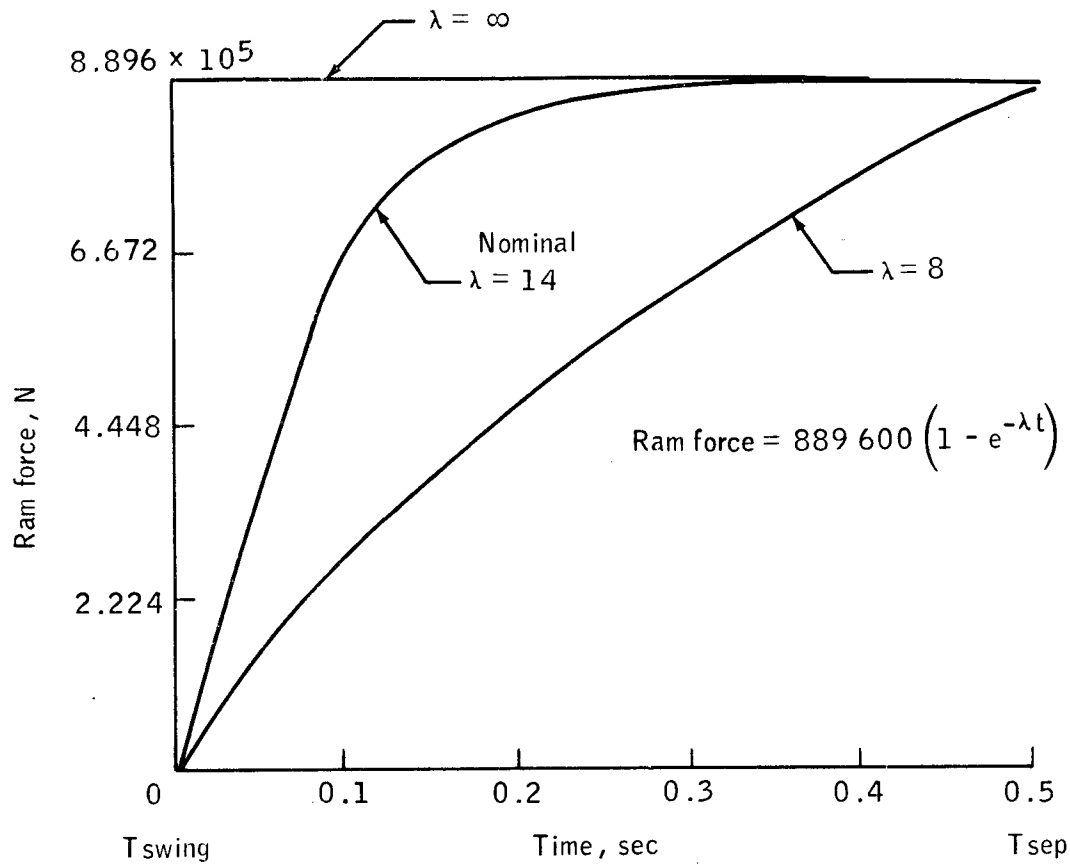

Figure 8.- Raw mechanism force scheduling.

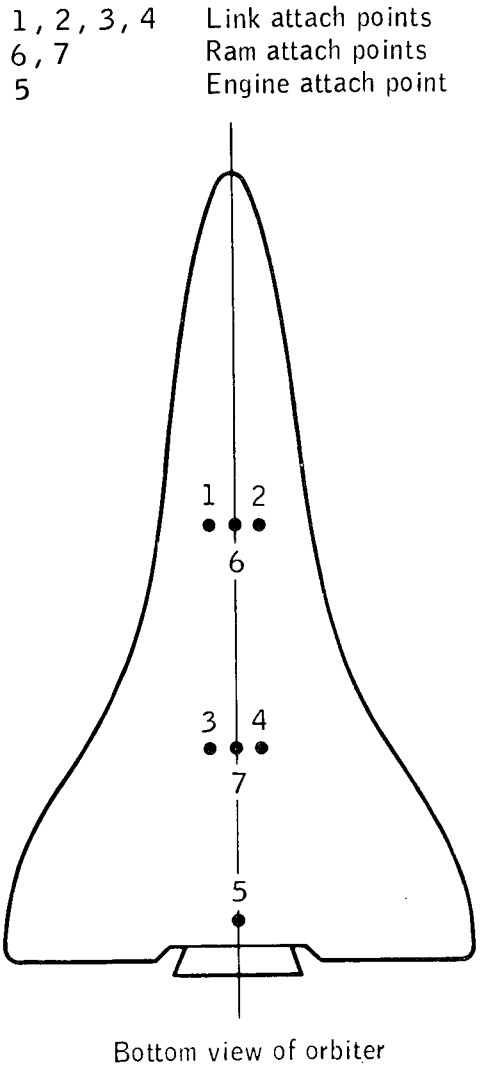

Figure 9. - Orbiter node points where external forces are applied.

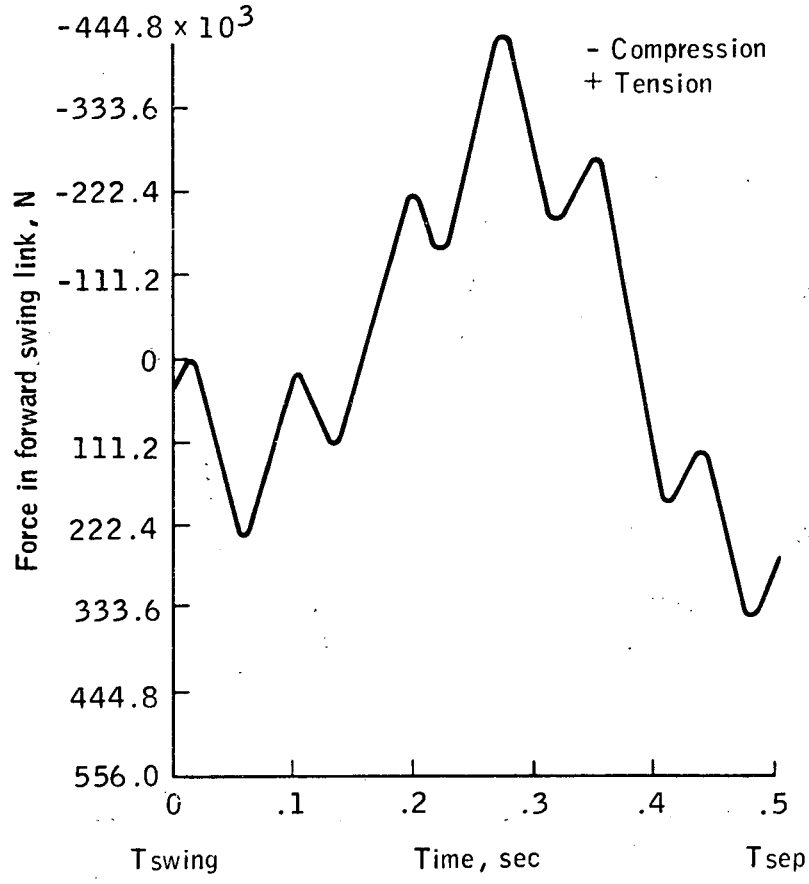

Figure 10. - Case 1, force in forward swing links.

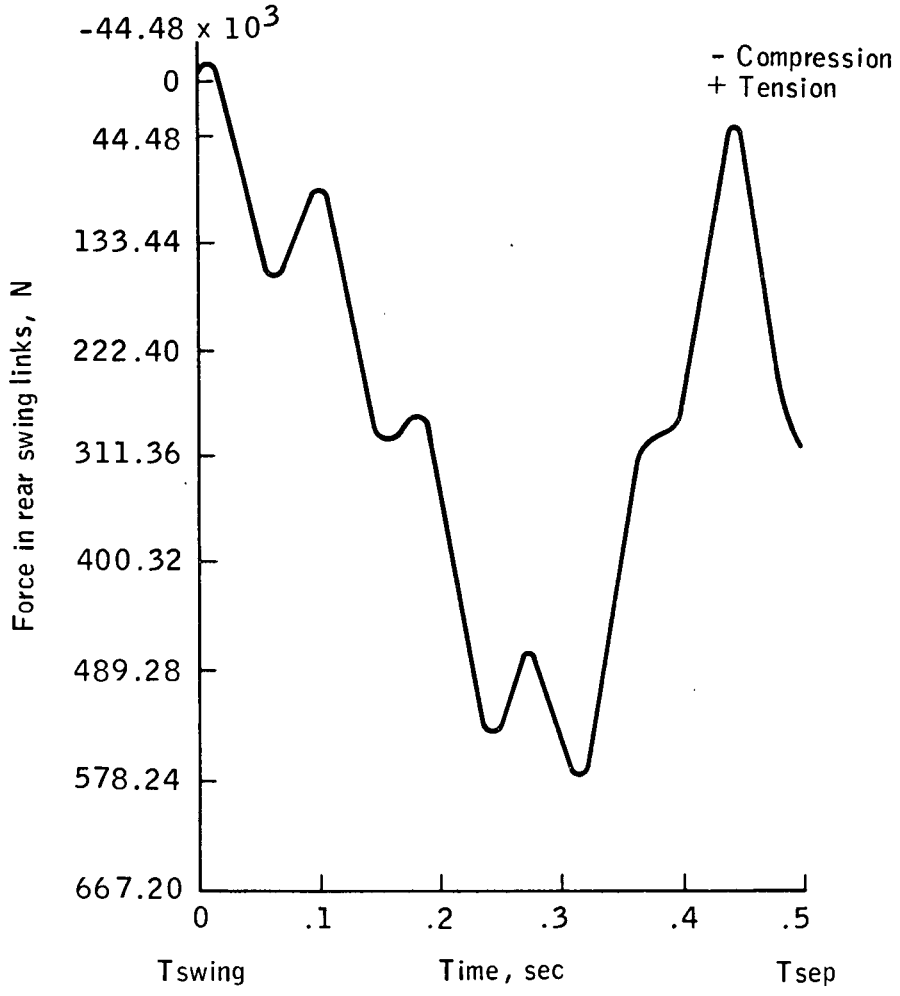

Figure 11.- Case 1, force in rear swing links.

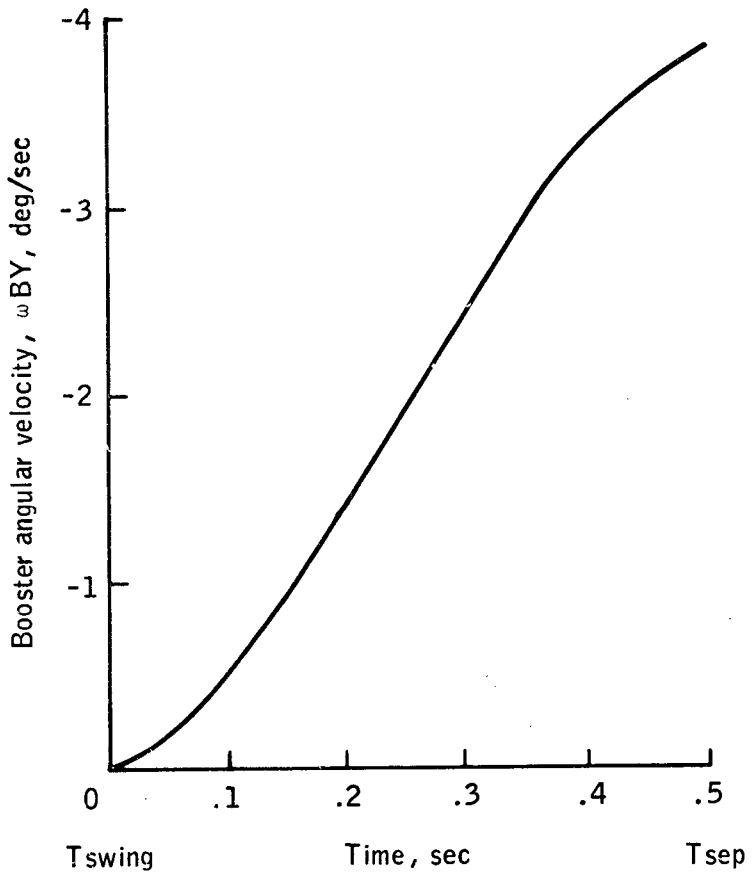

Figure 12.- Case 1, booster angular velocity.

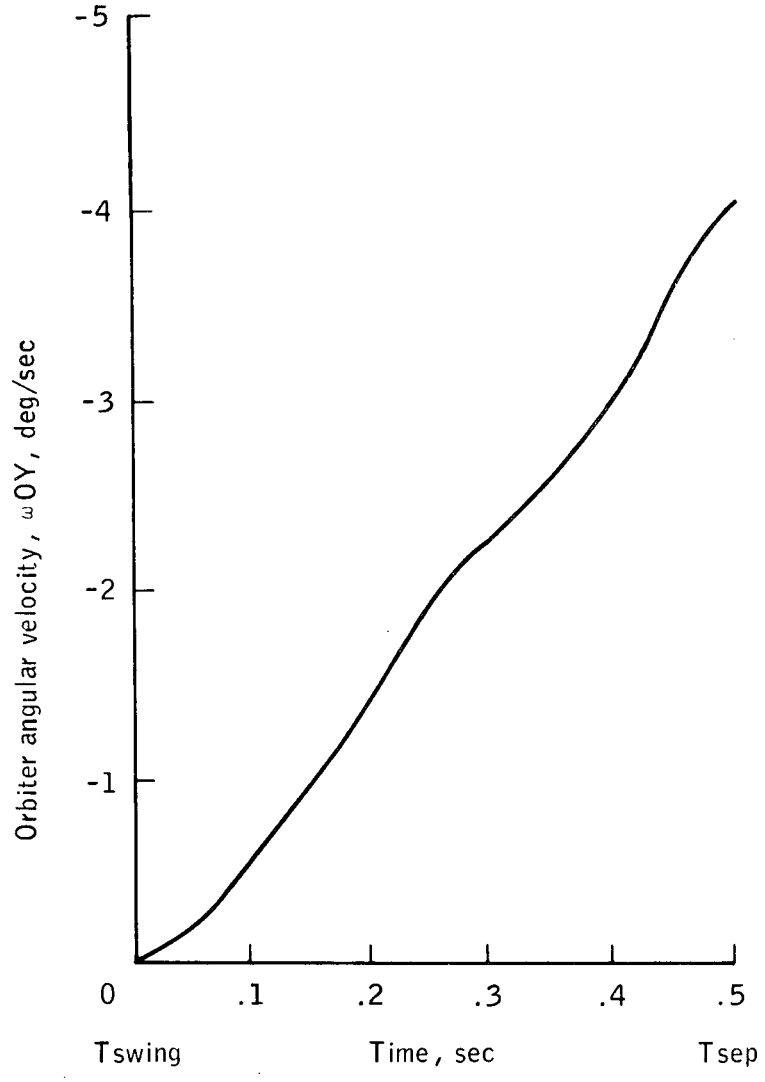

Figure 13.- Case 1, orbiter angular velocity.

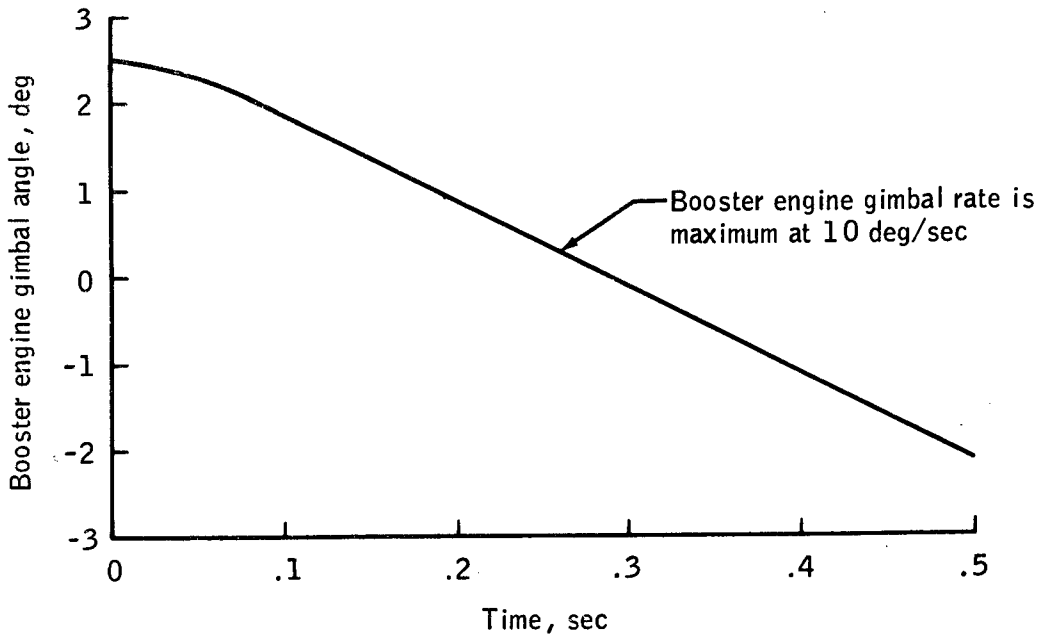

Figure 14.- Booster engine gimbal angle.

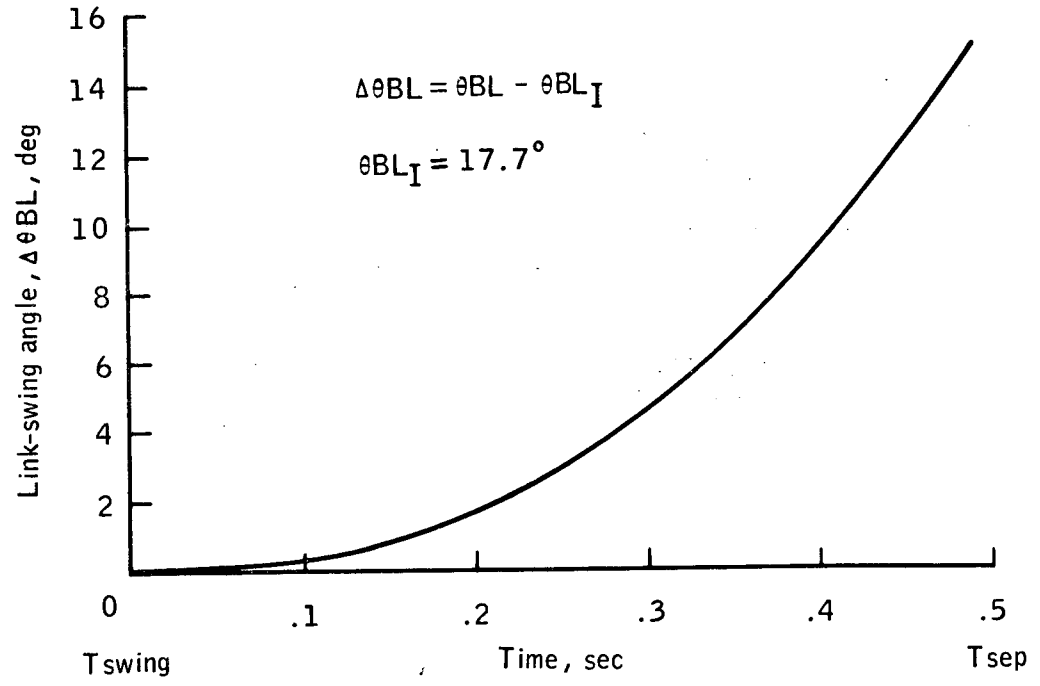

Figure 15.- Link-swing angle as compared to time.

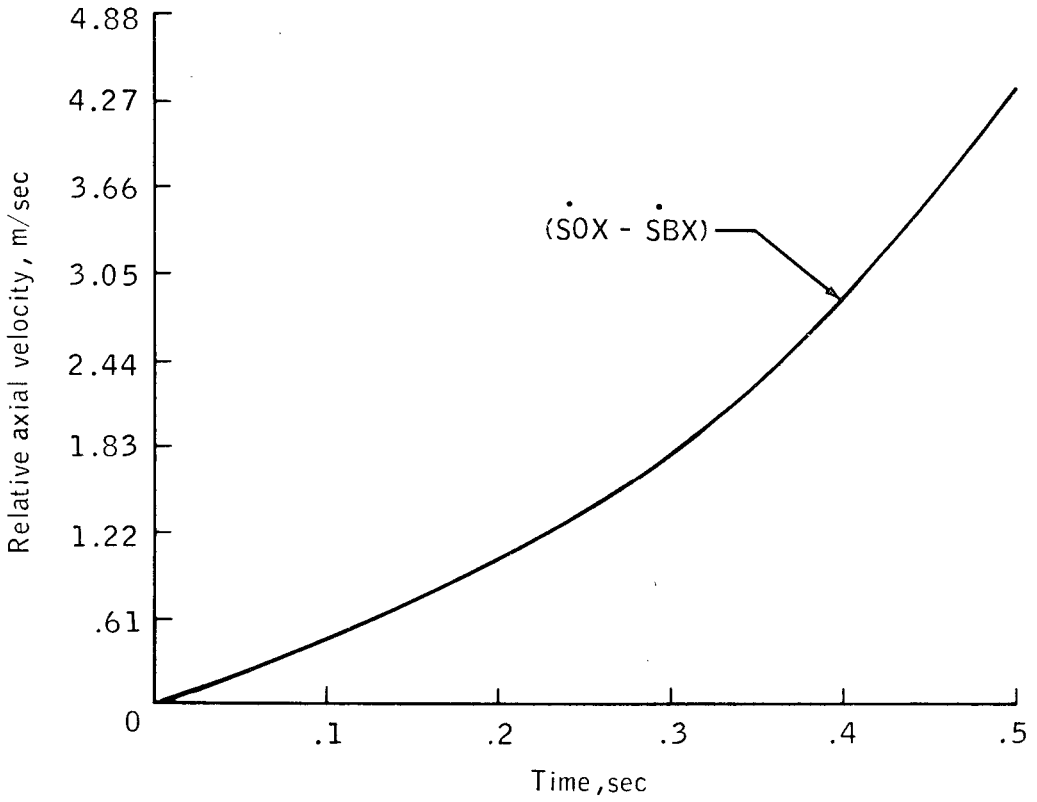

Figure 16. - Case 1, relative inertial axial velocity between booster and orbiter centers of gravity.

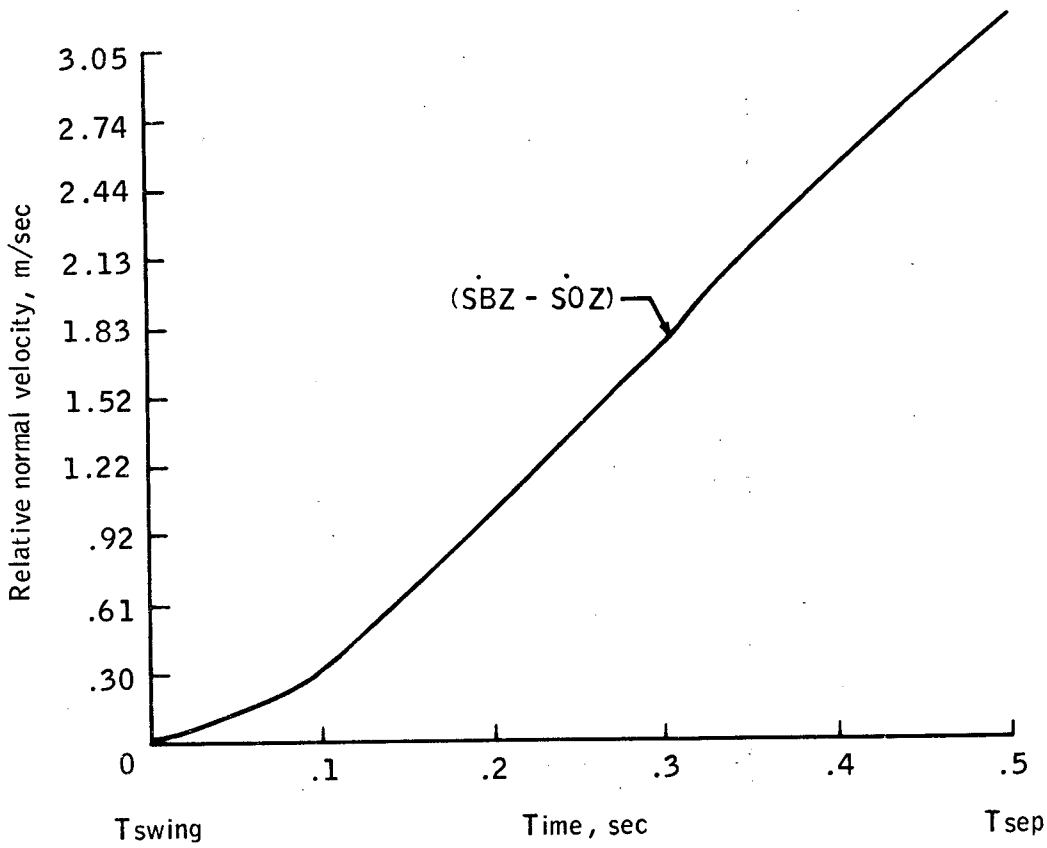

Figure 17.- Case 1, relative inertial normal velocity between booster and orbiter centers of gravity.

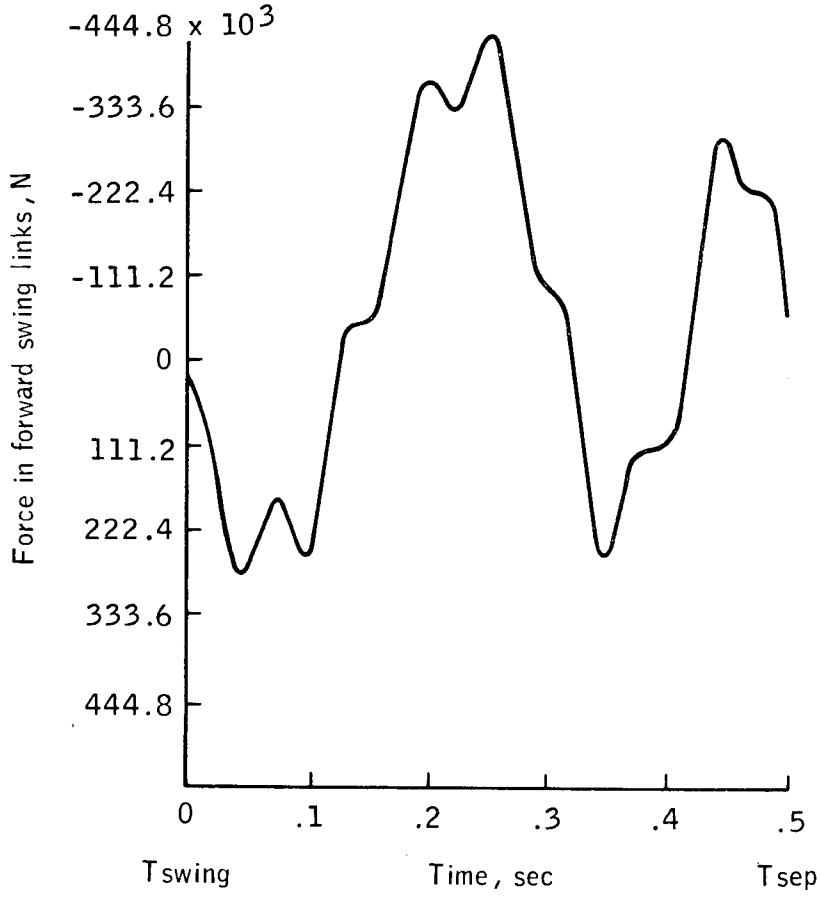

Figure 18.- Case 2, force in forward swing links.

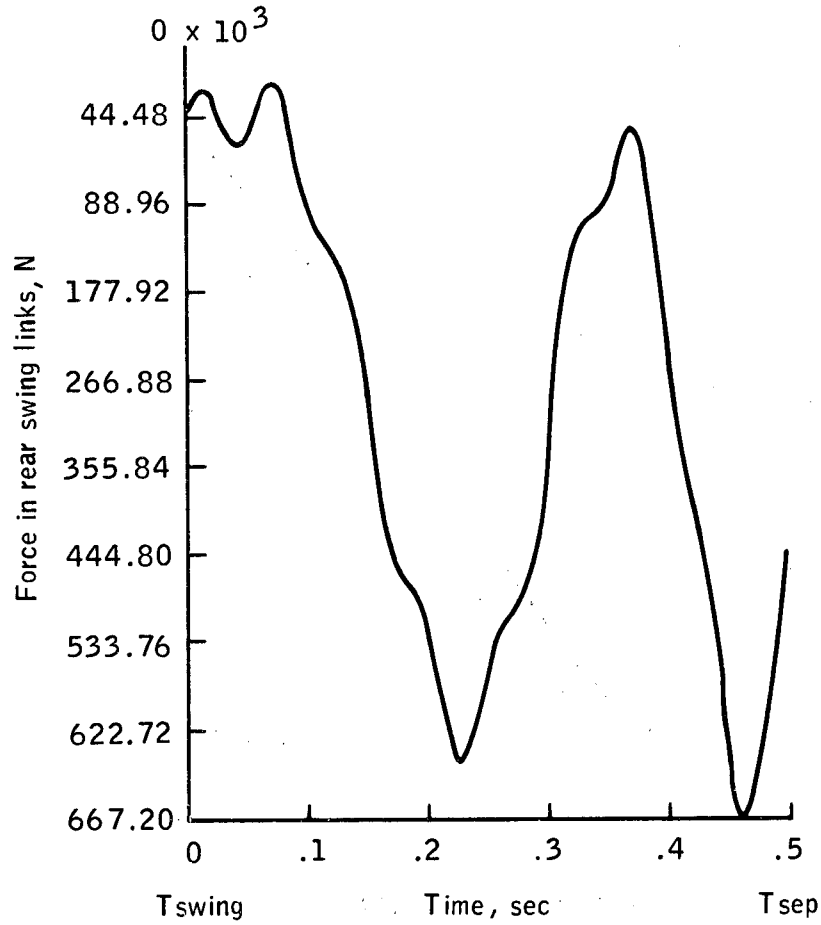

Figure 19.- Case 2, force in rear swing links.

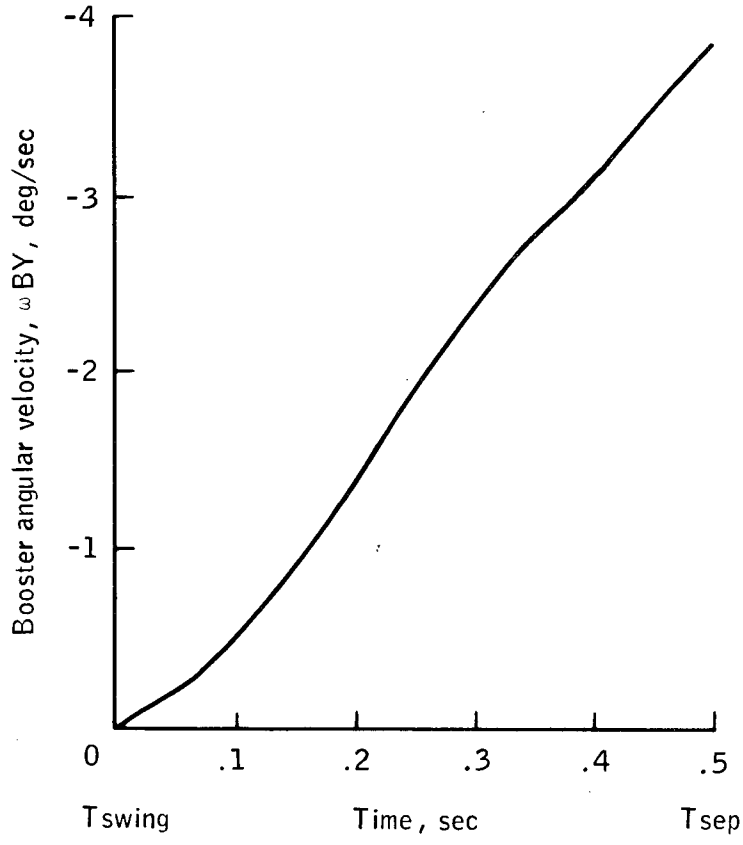

Figure 20. - Case 2, booster angular velocity.

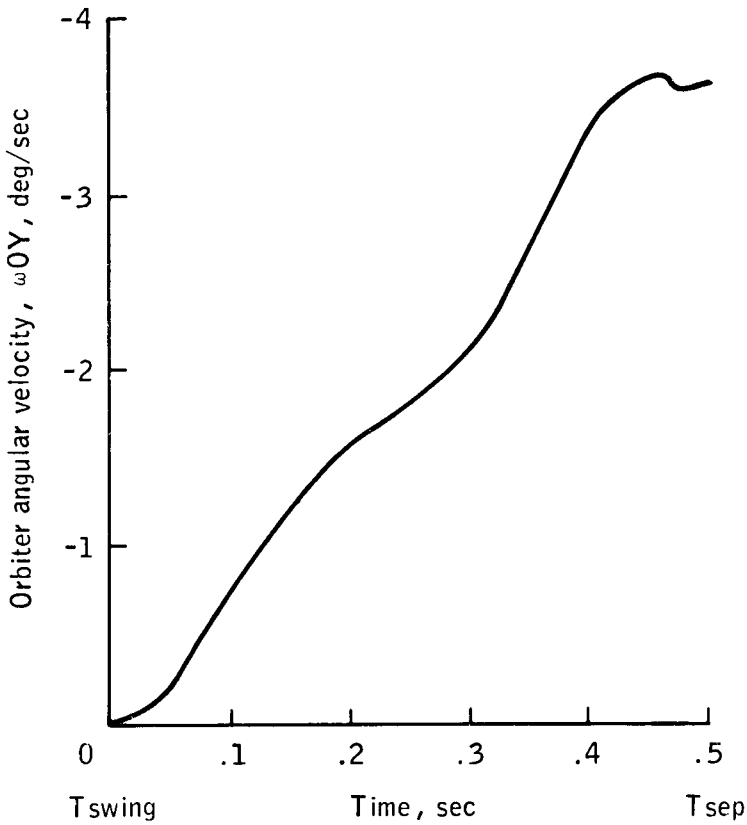

Figure 21.- Case 2, orbiter angular velocity.

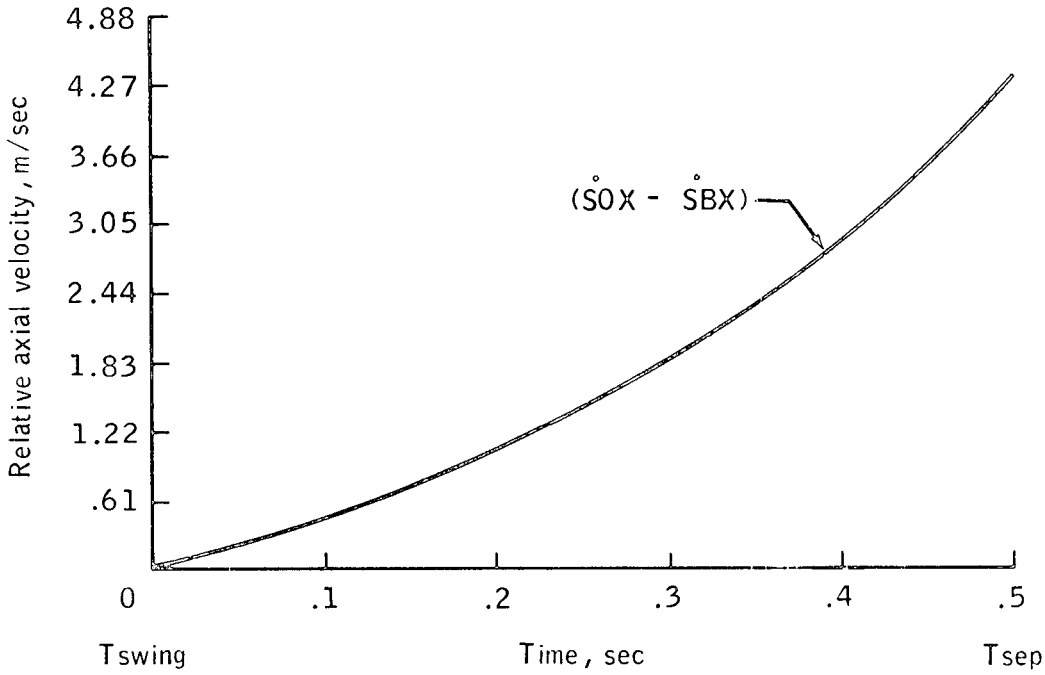

Figure 22. - Case 2, relative inertial axial velocity between booster and orbiter centers of gravity.

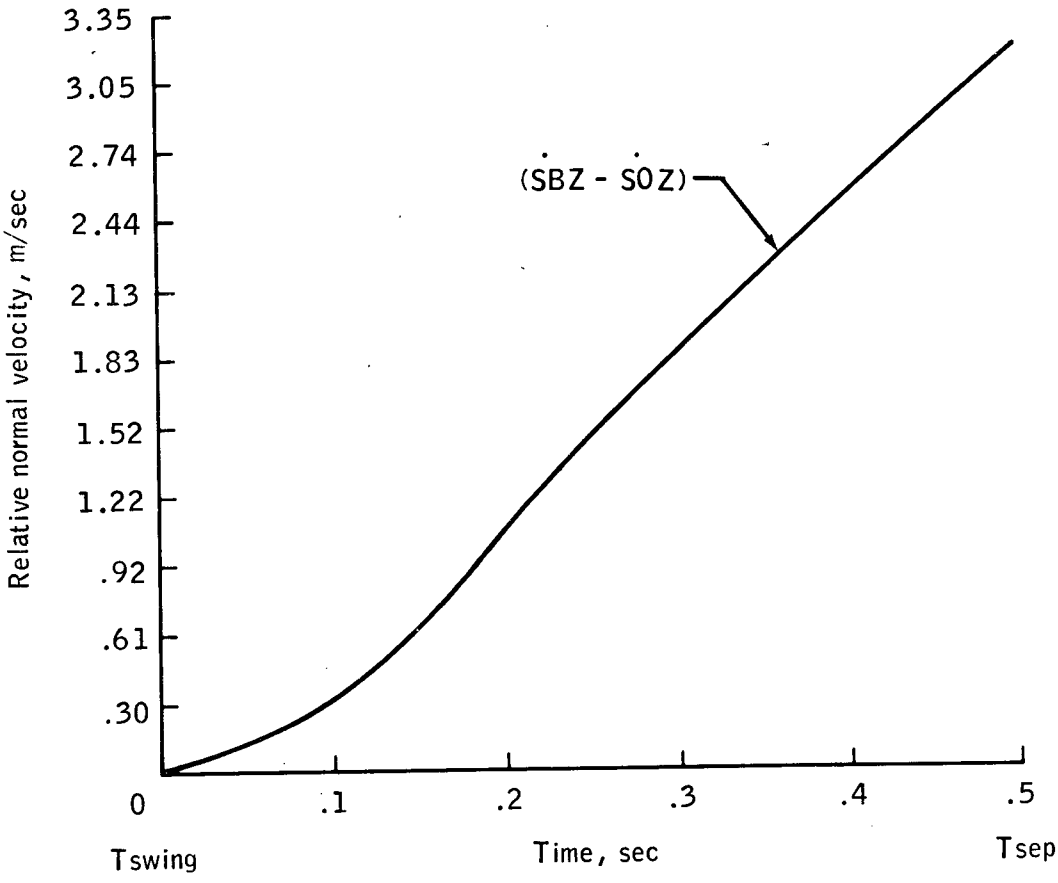

Figure 23.- Case 2, relative inertial normal velocity between booster and orbiter centers of gravity.

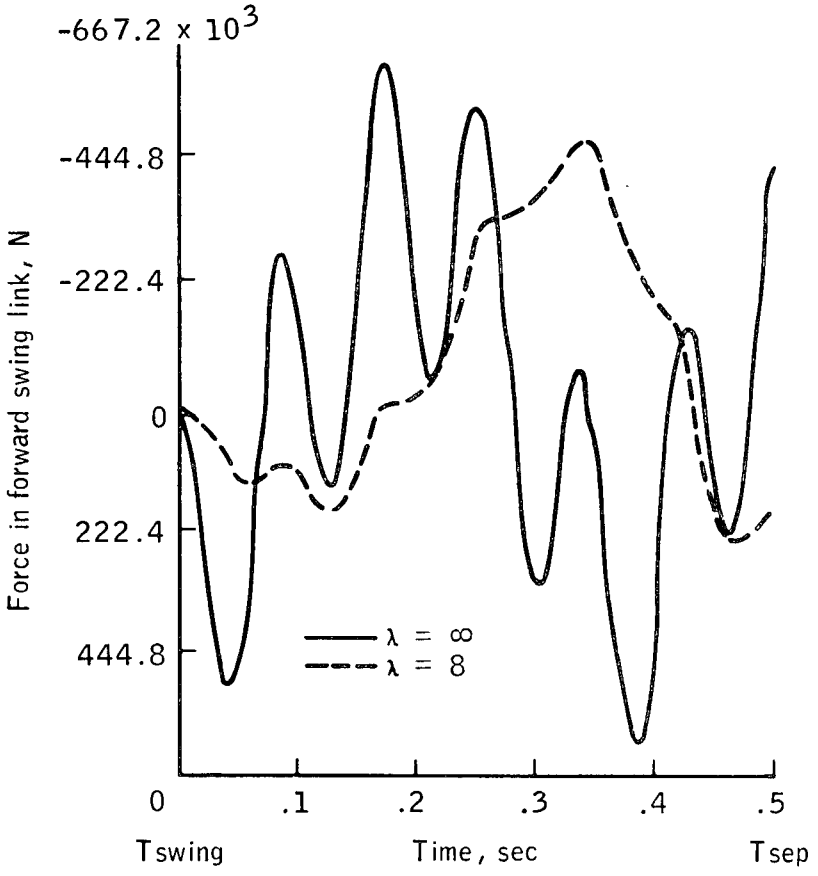

Figure 24.- Case 3, force in forward swing links.

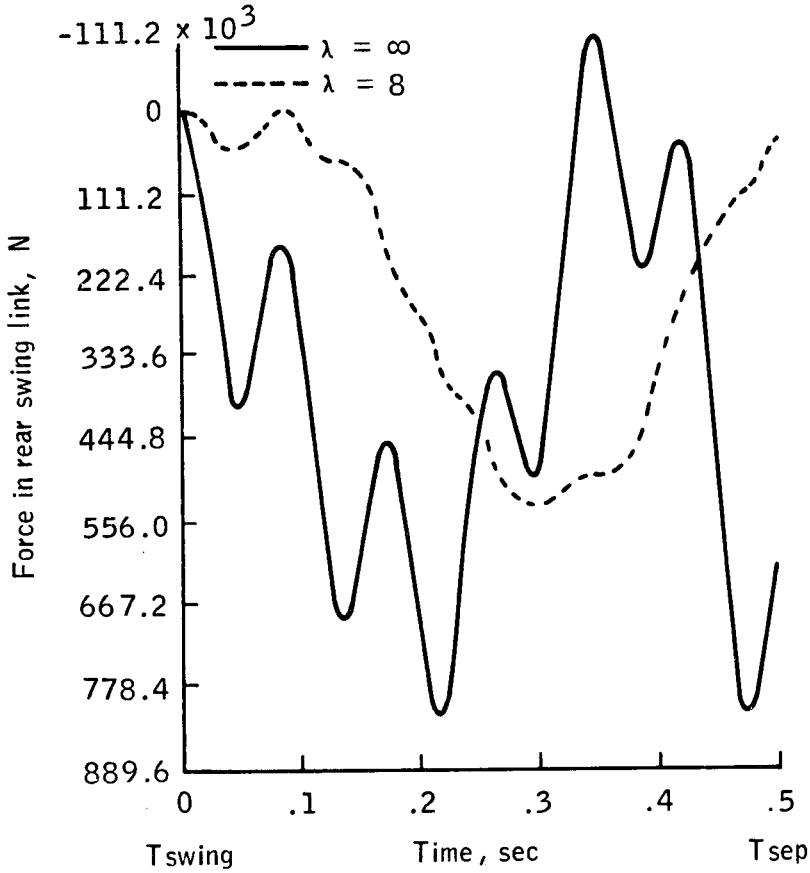

Figure 25.- Case 3, force in rear swing links.

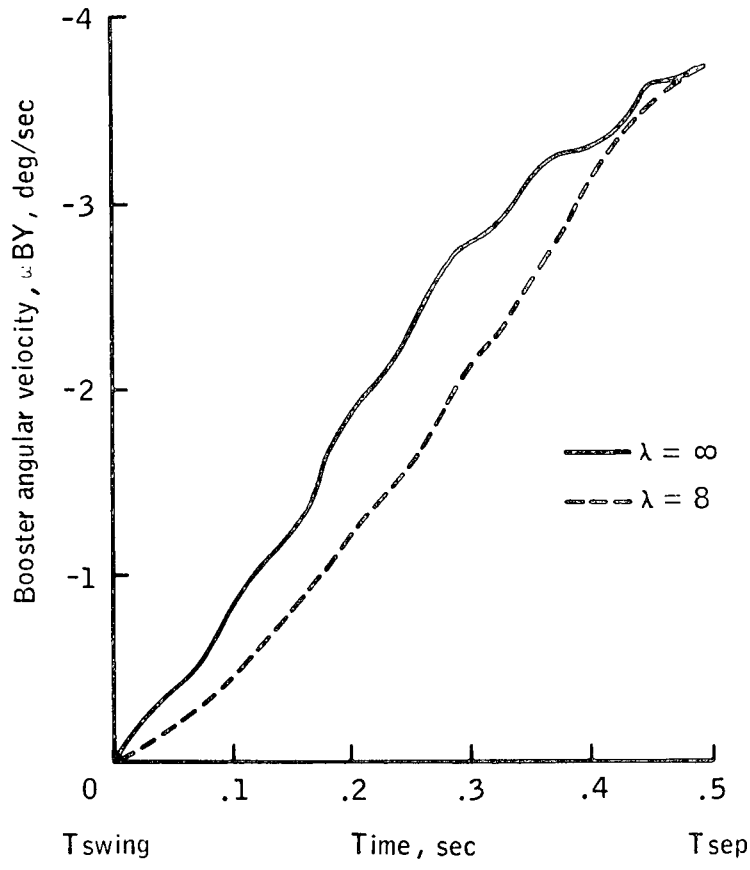

Figure 26.- Case 3, booster angular velocity.

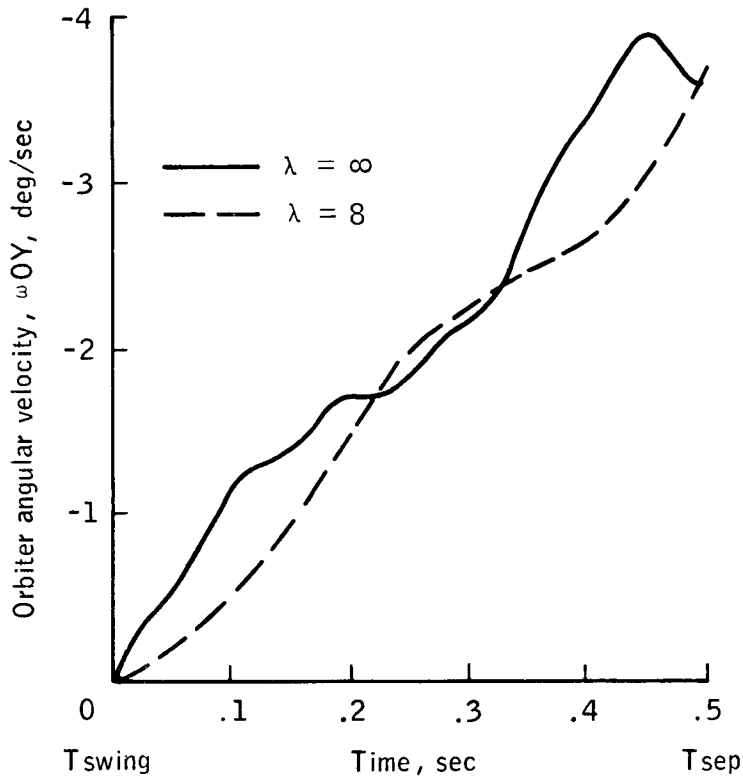

Figure 27.- Case 3, orbiter angular velocity.

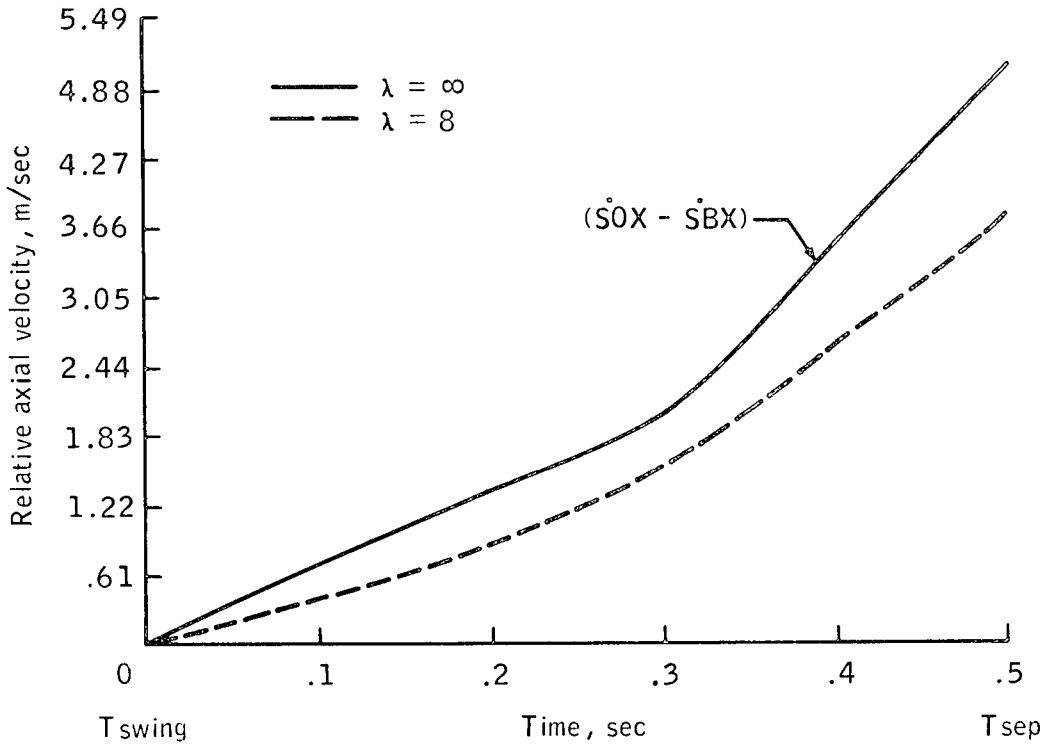

Figure 28. - Case 3, relative inertial axial velocity between booster and orbiter centers of gravity.

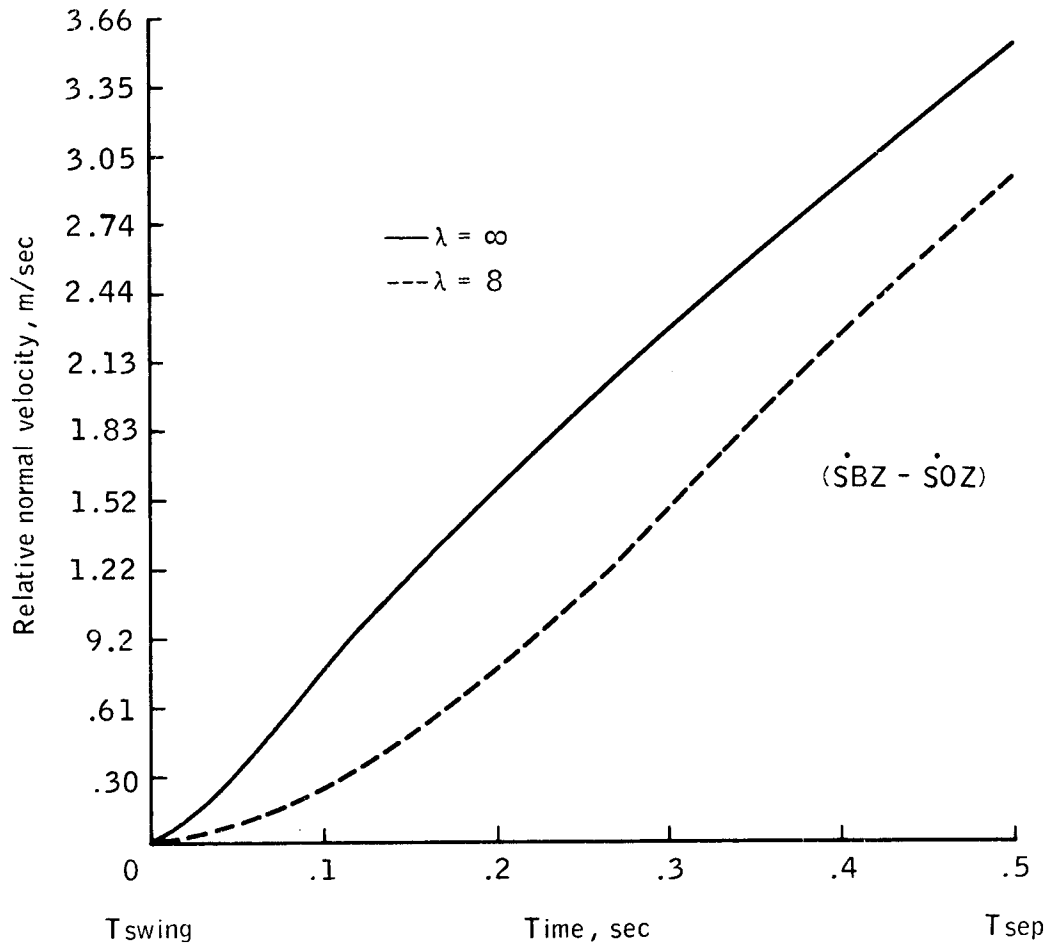

Figure 29.- Case 3, relative inertial normal velocity between booster and orbiter centers of gravity.

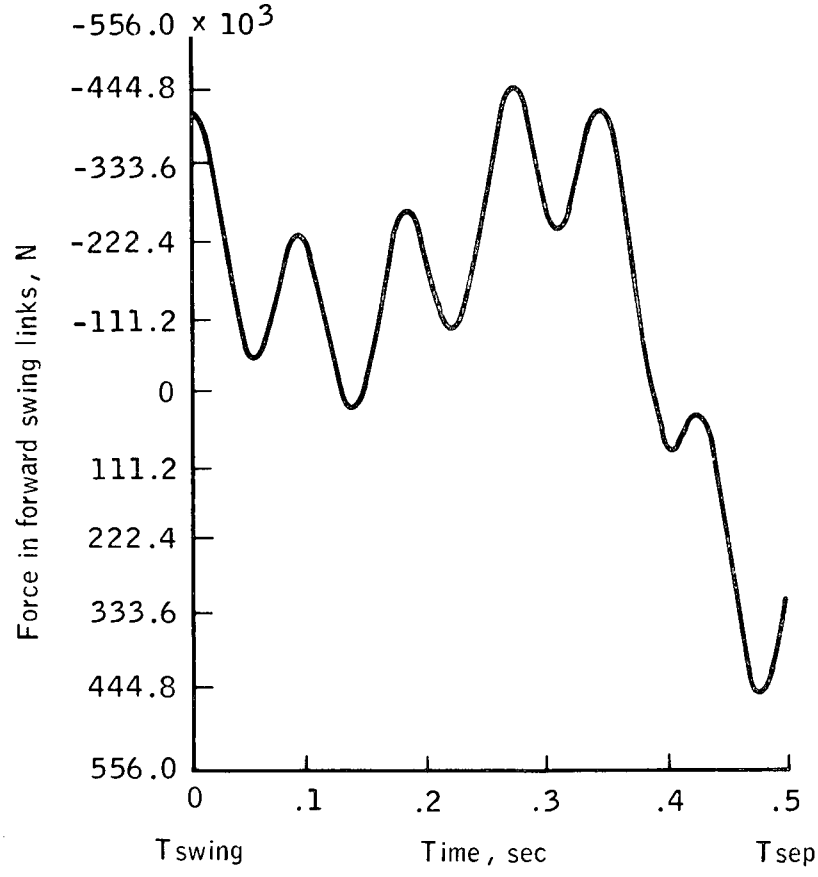

Figure 30.- Case 4, force in forward swing links.

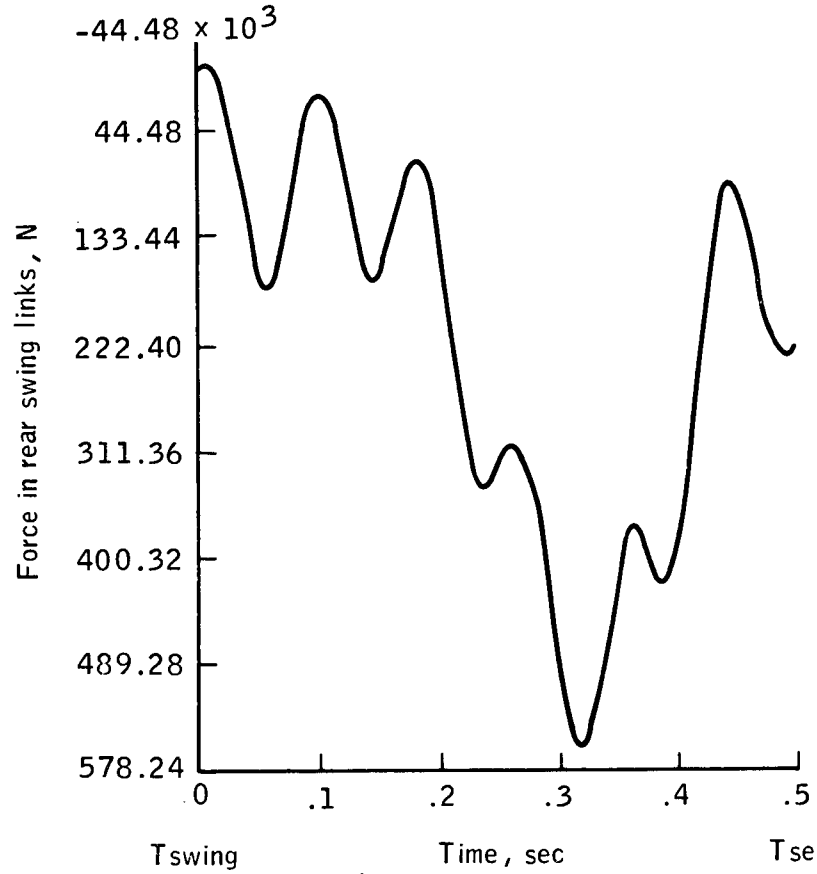

Figure 31.- Case 4, force in rear swing links.

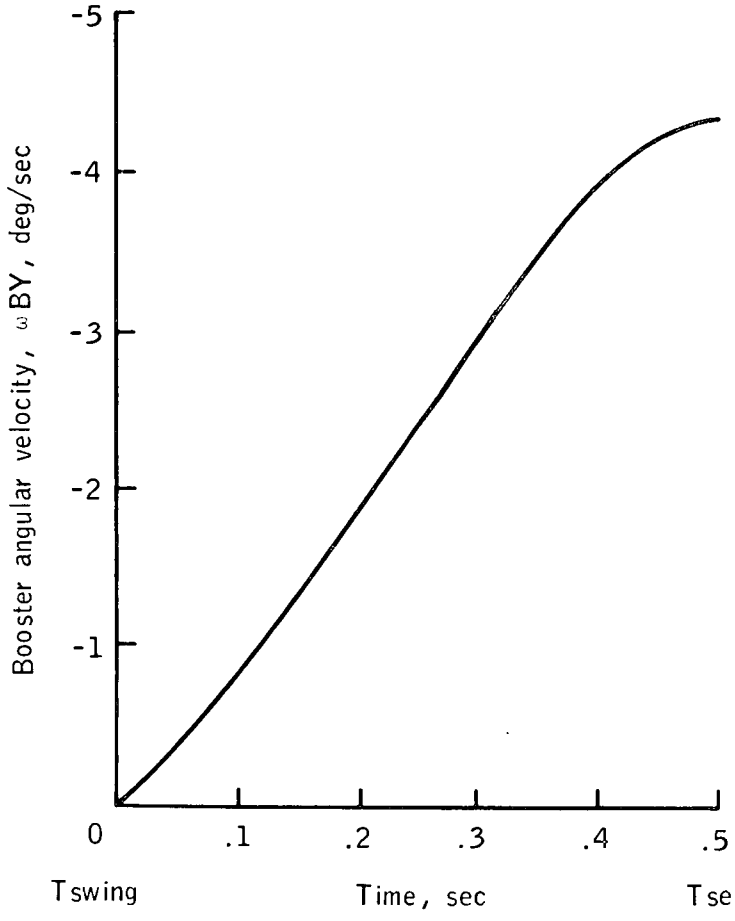

Figure 32.- Case 4, booster angular velocity.

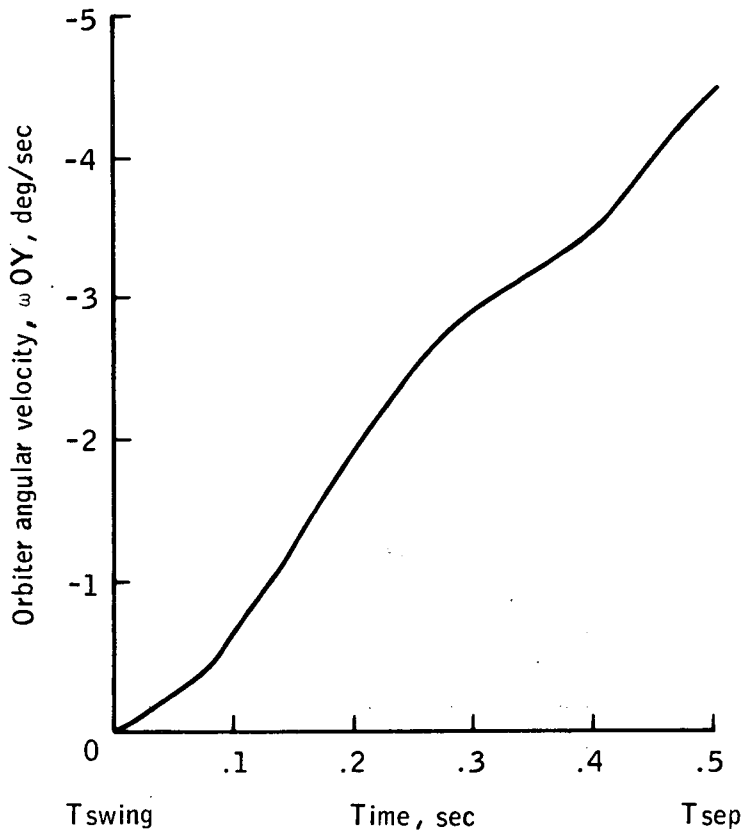

Figure 33.- Case 4, orbiter angular velocity.

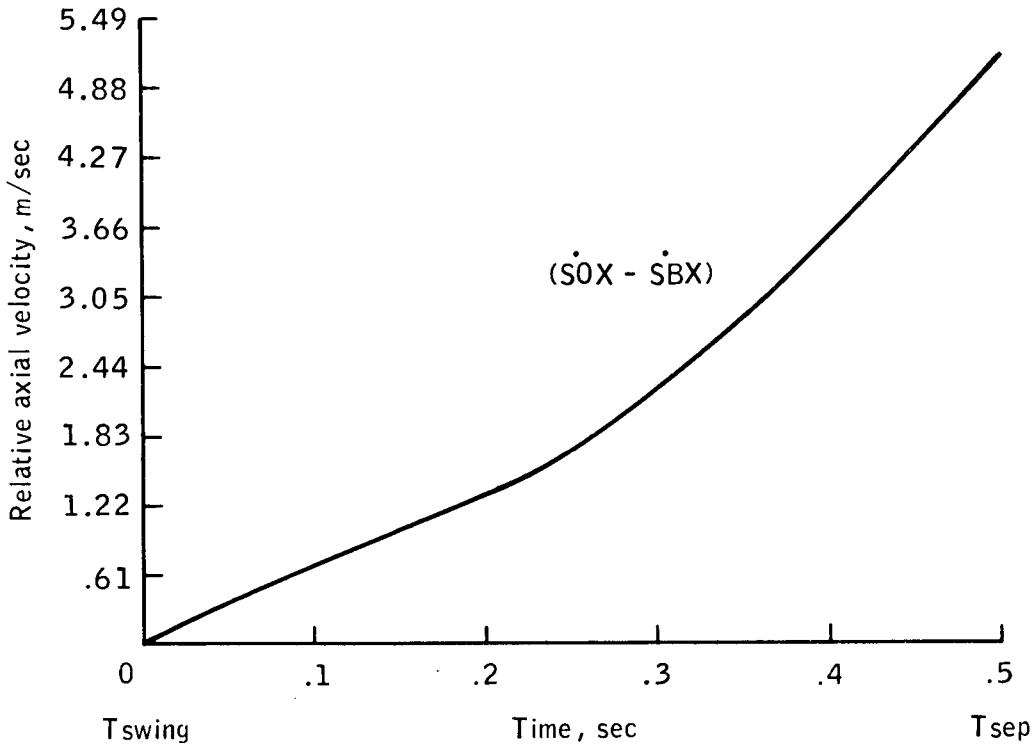

Figure 34. - Case 4, relative inertial axial velocity between booster and orbiter centers of gravity.

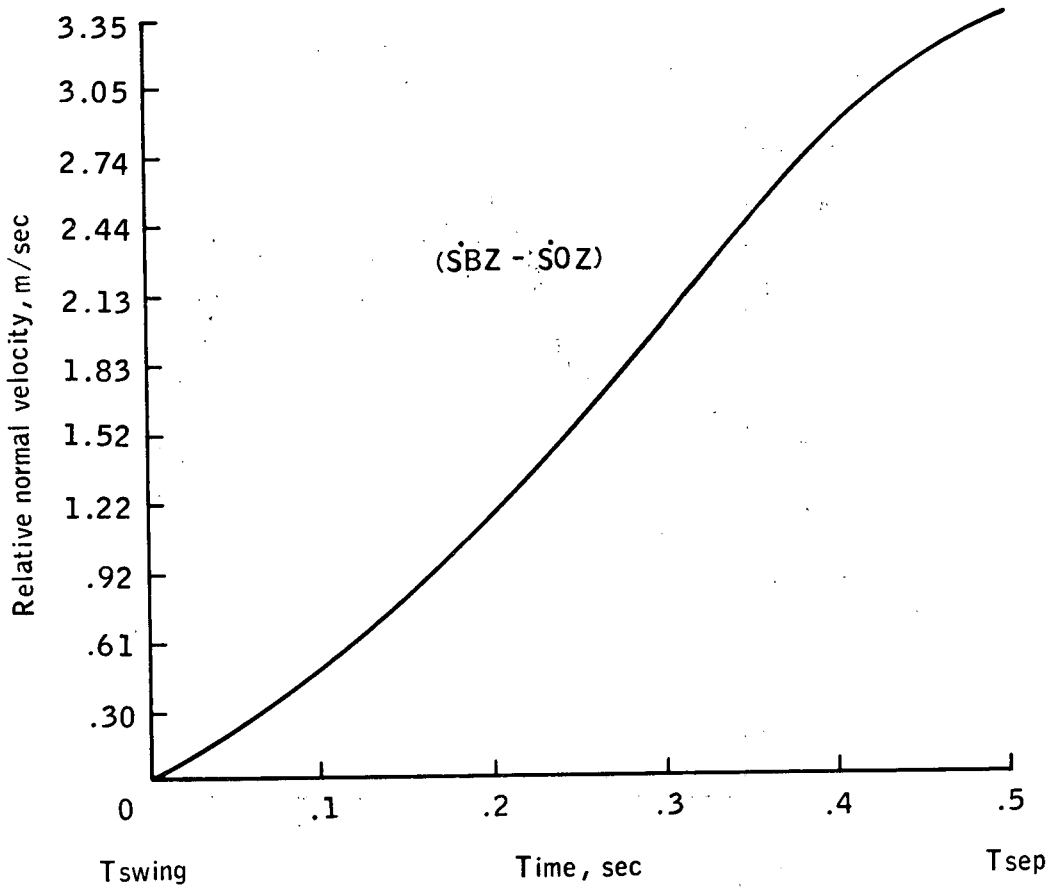

Figure 35. - Case 4, relative inertial normal velocity between booster and orbiter centers of gravity.

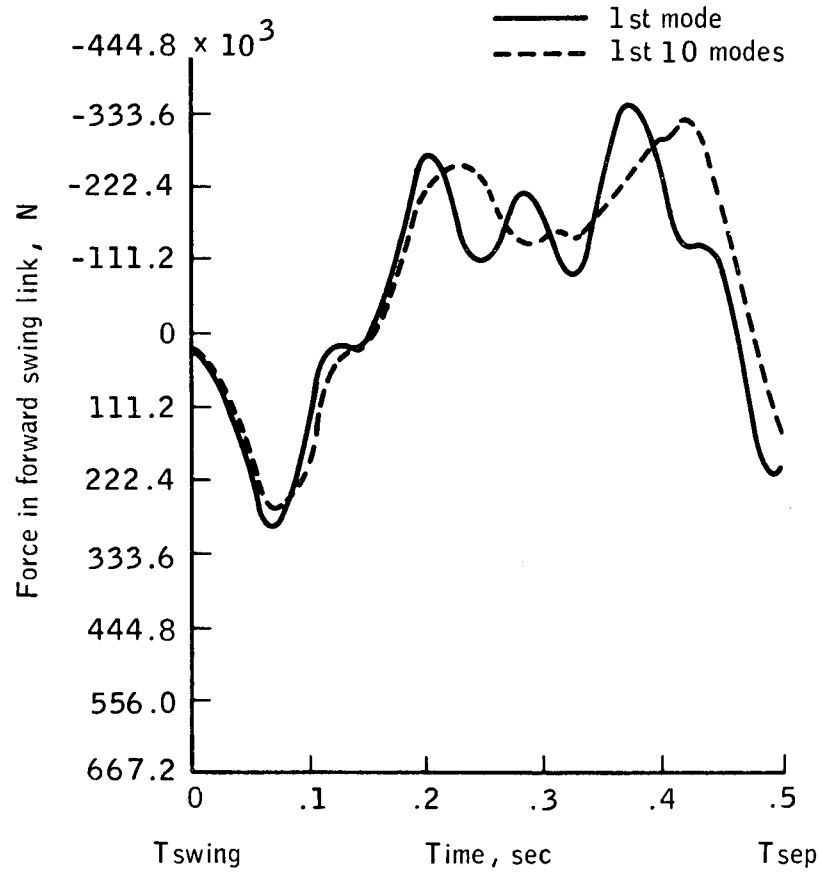

Figure 36.- Case 5, force in forward swing links.

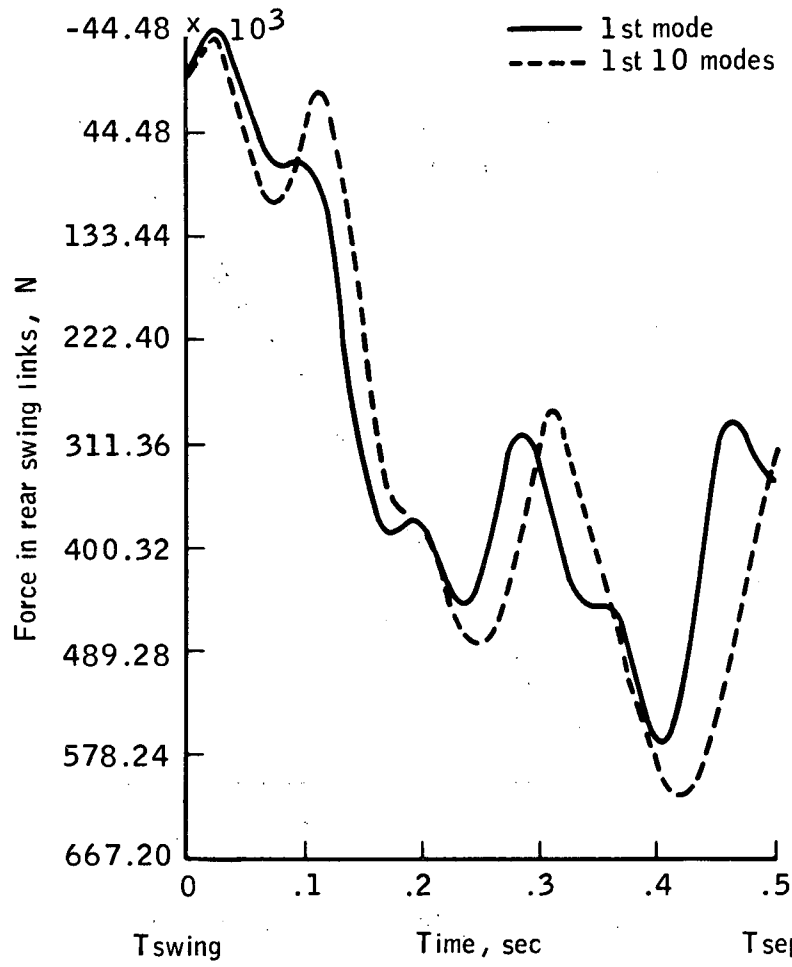

Figure 37.- Case 5, force in rear swing links.

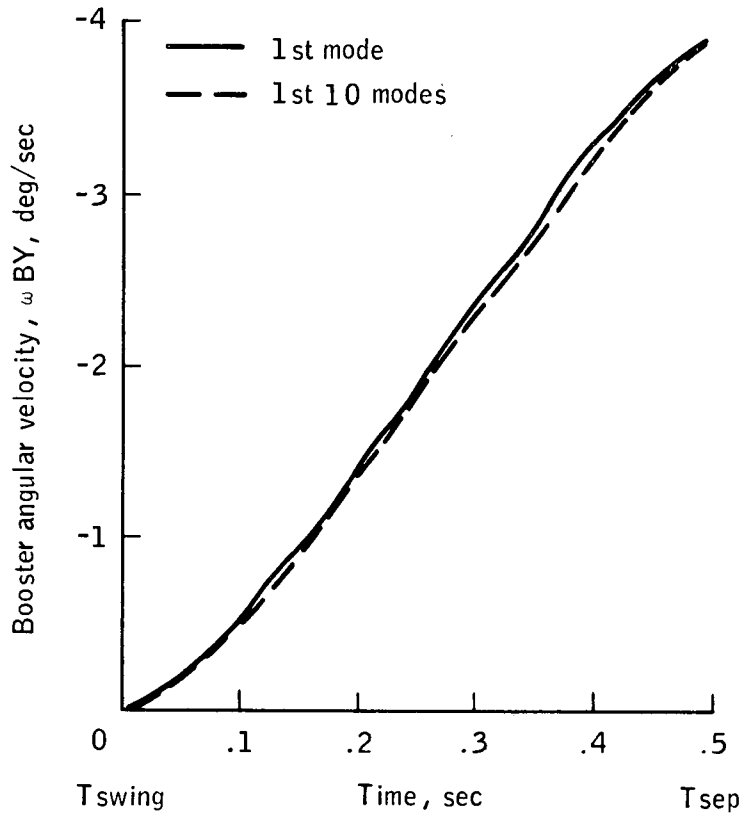

Figure 38. - Case 5, booster angular velocity.

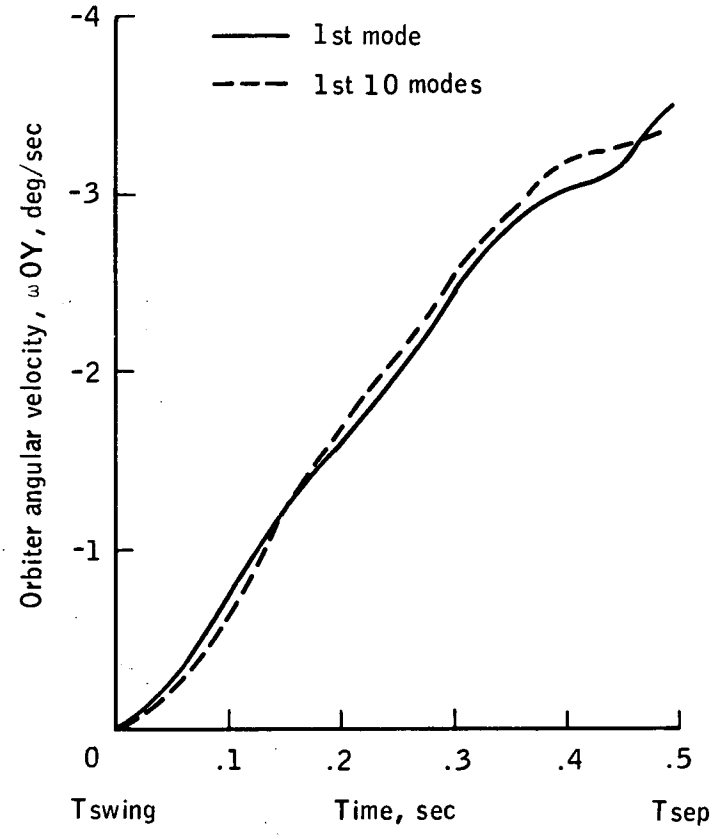

Figure 39. - Case 5, orbiter angular velocity.

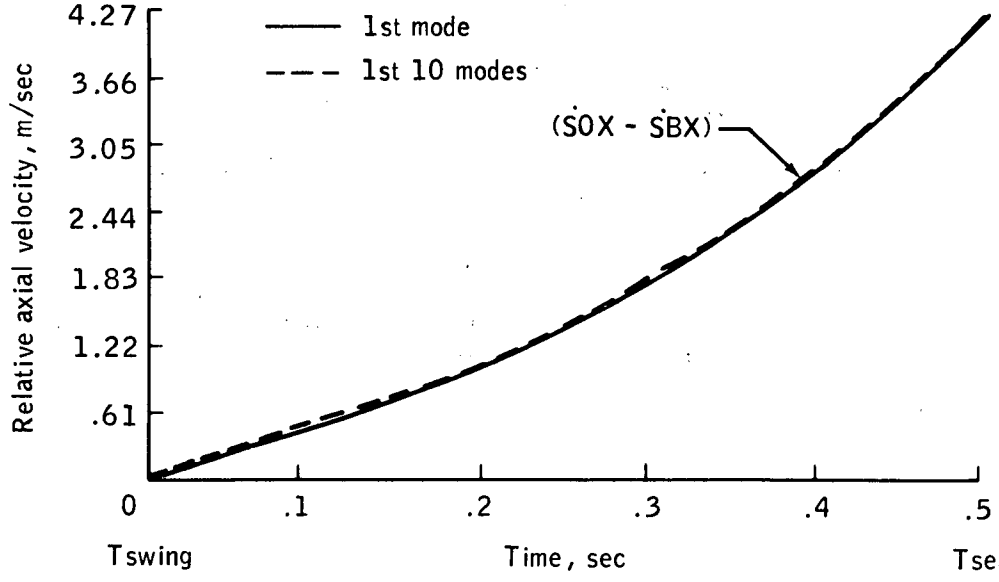

Figure 40. - Case 5, relative inertial axial velocity between booster and orbiter centers of gravity.

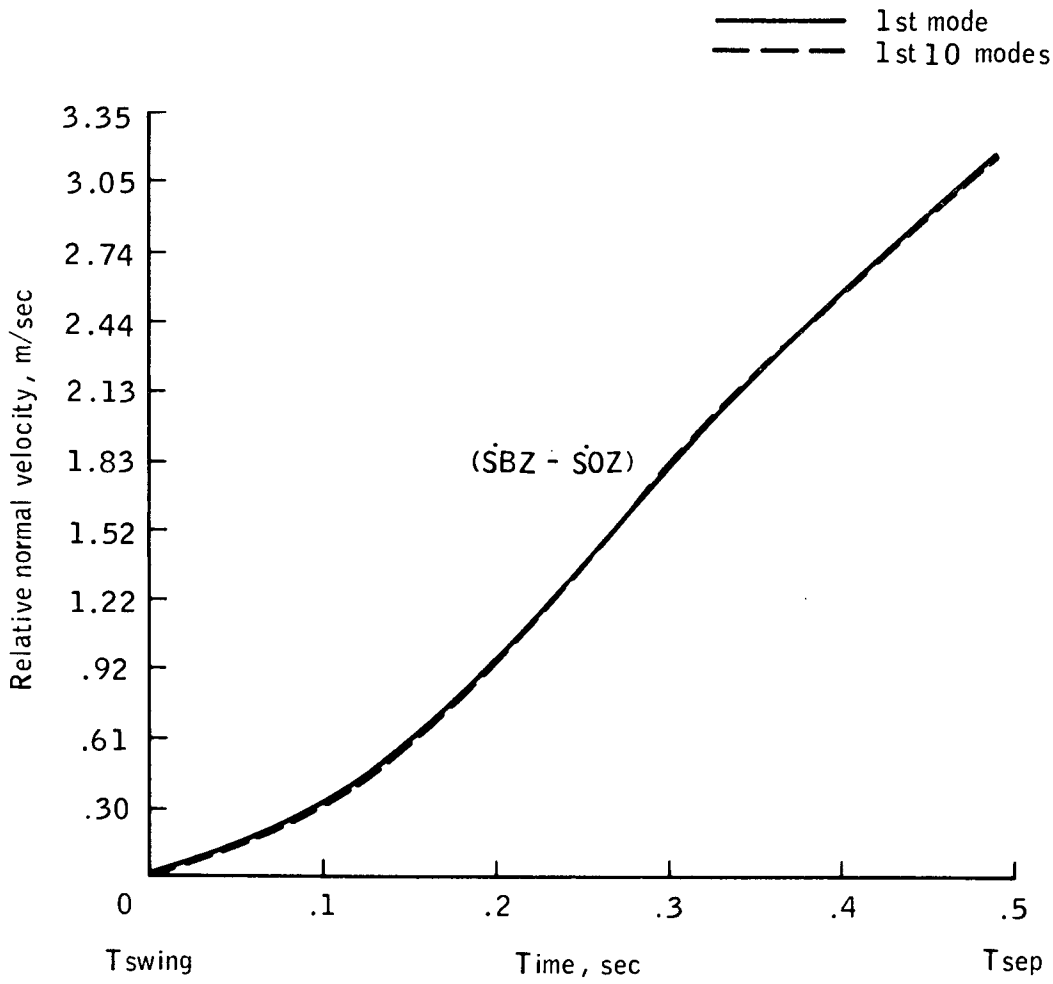

Figure 41.- Case 5, relative inertial normal velocity between booster and orbiter centers of gravity.

APPENDIX A

LINK STIFFNESS CALCULATIONS

The link stiffness calculations are made by idealizing each link member as a beam element. The general stiffness for a beam element that undergoes a full six-degree-of-freedom deflection at each end is derived in reference 4. The link element boundary conditions can be applied to the general beam stiffness matrix so that the link stiffness matrix can be formulated. These boundary conditions are that each link member is pinned at its end points with the pin parallel to the Y_L-axis (fig. A-1). The deflections and forces that correspond to the link element boundary conditions, as illustrated in figure A-1, are related by the link stiffness matrices; that is,

$$\begin{Bmatrix} F1 \\ F2 \\ T4 \\ T6 \\ F7 \\ F8 \\ T10 \\ T12 \end{Bmatrix} = \begin{bmatrix} AE/\ell & & & & & & & \\ 0 & 12EI/\ell^3 & & & & \text{Symmetric} & & \\ 0 & 0 & JG/\ell & & & & & \\ 0 & 6EI/\ell^2 & 0 & 4EI/\ell & & & & \\ -AE/\ell & 0 & 0 & 0 & AE/\ell & & & \\ 0 & -12EI/\ell^3 & 0 & -6EI/\ell^2 & 0 & 12EI/\ell^3 & & \\ 0 & 0 & -JG/\ell & 0 & 0 & 0 & JG/\ell & \\ 0 & 6EI/\ell^2 & 0 & 2EI/\ell & 0 & -6EI/\ell^2 & 0 & 4EI/\ell \end{bmatrix} \begin{Bmatrix} U1 \\ U2 \\ U4 \\ U6 \\ U7 \\ U8 \\ U10 \\ U12 \end{Bmatrix} \tag{A-1}$$

where A is the link element cross-sectional area, I is the cross-sectional moment of inertia, J is the polar moment of inertia, E is the modulus of elasticity, G is the shear modulus of elasticity, and ℓ is the link element.

For simplification, the deflections of link end II (fig. A-1) are calculated relative to end I. Thus, the matrix equation (A-1) can be rewritten for $U_1 = U_2 = U_4 = U_6 = 0$, that is,

$$\begin{Bmatrix} F7 \\ F8 \\ T10 \\ T12 \end{Bmatrix} = \begin{bmatrix} AE/\ell & 0 & 0 & 0 \\ 0 & 12EI/\ell^3 & 0 & -6EI/\ell^2 \\ 0 & 0 & JG/\ell & 0 \\ 0 & -6EI/\ell^2 & 0 & 4EI/\ell \end{bmatrix} \begin{Bmatrix} U7 \\ U8 \\ U10 \\ U12 \end{Bmatrix} \tag{A-2}$$

and

$$\begin{Bmatrix} F1 \\ F2 \\ T4 \\ T6 \end{Bmatrix} = -\begin{Bmatrix} F7 \\ F8 \\ T10 \\ T12 \end{Bmatrix} + \begin{Bmatrix} 0 \\ 0 \\ 0 \\ F2 \cdot \ell \end{Bmatrix} \tag{A-3}$$

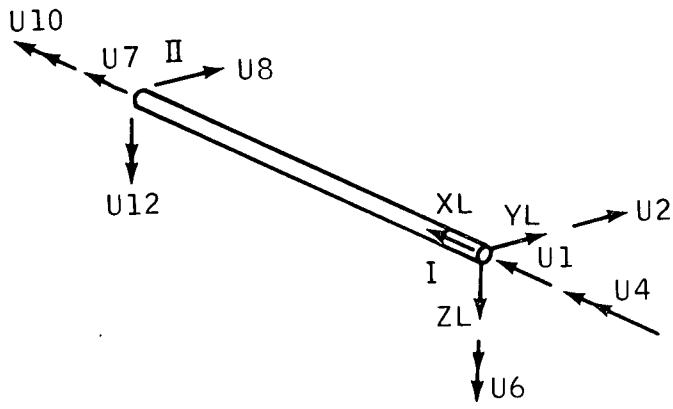

(a) Beam forces.

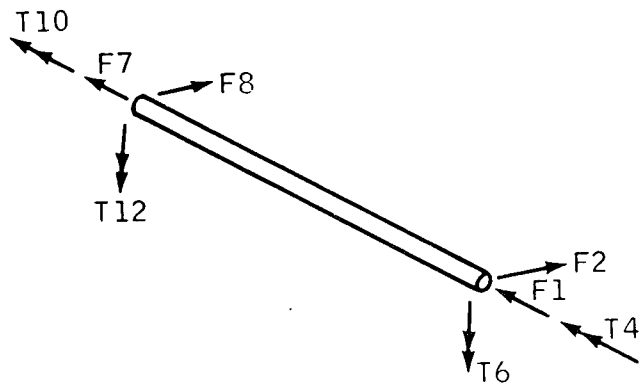

(b) Beam deflections.

Figure A-1.- Beam deflections and beam forces.

APPENDIX B

COMPUTER PROGRAM

The mathematical model developed in the previous chapters was incorporated into a computer program so that the staging maneuver could be simulated as a function of time. The program was written in FORTRAN V language and was run on the UNIVAC 1108 digital computer. The numerical integration routine used in the program was a variable step size Adams-Moulton method utilizing a fourth-order Runge-Kutta procedure for the required starting values. A description of the integration procedure is presented in reference B-1.

REFERENCE

B-1. Hildebrand, F. B.: Introduction to Numerical Analysis. McGraw-Hill Book Co., Inc., 1956.